THE UNIVERSITY OF MICHIGAN
COLLEGE OF ENGINEERING
Department of Nuclear Engineering

Progress Report
May 1, 1961-May 1, 1962

NEUTRON OPTICS

P. F. Zweifel

Report Prepared by:

J. S. King
J. Donovan
W. Myers

With Contributions from:

K. Carpenter
E. Straker

ORA Project 03671

under contract with:

NATIONAL SCIENCE FOUNDATION
GRANT NO. G-12147
WASHINGTON, D.C.

administered through:

OFFICE OF RESEARCH ADMINISTRATION ANN ARBOR

July 1962

TABLE OF CONTENTS

LIST OF ILLUSTRATIONS

LIST OF ILLUSTRATIONS (Concluded)

A. FOREWORD

This is the second annual Progress Report on "Neutron Optics," an experimental project sponsored by the National Science Foundation under Grant No. G-21247, effective May 1, 1960 to April 30, 1963. It reviews work completed or undertaken between May 1, 1961 and May 1, 1962. As described in the first annual Progress Report, the project is devoted almost exclusively to the construction and operation of a triple-axis crystal spectrometer, used at the Ford Nuclear Reactor, Phoenix Memorial Laboratory, for the observation of elastic and inelastic scattering of thermal neutrons in solids and liquids.

Because of budget limitations, the project was reduced in staff during the year. The current personnel are:

(1) Over-all Responsibility (1/8 time)—P. F. Zweifel, Professor, Nuclear Engineering Department.

(2) Direct Supervision and Principal Investigator (1/2 time)—J. S. King, Professor, Nuclear Engineering Department.

(3) Detection Systems, Crystal Monochromator Studies (1/2 time)—William Myers, graduate student, Nuclear Engineering Department.

(4) Spectrometer Assembly, Calibration, Initial Experimenter (full time)—John Donovan, doctoral candidate, Nuclear Engineering Department.

(5) Crystal Growing (1/8 time)—George Wang, graduate student, School of Public Health.

Part of the support for mechanical design and construction has been provided without charge by the Nuclear Engineering Department, and part has been provided on a paid hourly basis by personnel outside the Department. Ninety percent of the financial support for John Donovan has come from outside sources.

B. SYNOPSIS OF PROGRAM AND PROGRESS

The goals set forth one year ago have largely been achieved in this report period. The construction phase is completed, initial intensity and calibration of the triple-axis scattering system has been accomplished, and an initial scattering experiment on solid C_nH_{2n} has been underway since April, 1961. The signal and background levels predicted a year ago have been approximately realized, although the levels are marginal, as anticipated. Studies of relative reflecting properties for various monochromating crystals have been conducted and initial results are included in this report. Progress in crystal growing techniques and in the optimization of reactor-leakage flux has been poor; because of budget limitations, little student effort could be expended in these directions.

Specific results are noted in the following paragraphs:

(1) Mechanical Construction: The triple-axis system is completed and operating. As shown in Figs. 1 and 2, this system includes a main turret, a main Bragg arm, a crystal table with a 2: 1 drive, a target table, a scattering-angle arm, a second Soller collimator, a second monochromating crystal table with shield housing, a second Bragg arm, and a Bragg detector with shielding.

(2) Automatic Spectrometer Drives: Independent gear drives for the main Bragg arm, scattering arm, and scattering table have been mounted and operated. These are driven by three d-c impulse motors which are manually operated at present. The motion of the motor is digitized and will soon be operated by a preset program for constant-momentum transfer, constant-energy transfer, or arbitrary combinations of these.

(3) Fast Neutron Shielding: The original shielding design included a large flexible water bag behind the turret. This proved impractical and has been replaced by a large water shield yoke which encloses the rear of the rotating turret, as shown in Fig. 2. Background measurements show that the two shields are essentially equivalent.

(4) Cu Crystal Monochromators: Two halves of a 3-in. (diameter) x 6-1/2-in. single copper crystal were purchased, their properties were measured, and they were put into operation for the first and second Bragg monochromatizations. For each section, the single-crystal rocking curve width (FWHM) was found to be approximately 9 min of arc, less than half the value anticipated. However, the peak reflection intensity for each section is comparable to that of all other crystals so far observed except beryllium. The consequence is a mismatch with

present collimator geometry but a better resolution than anticipated without much loss in intensity.

(5) Energy Resolution: The over-all triple-scattering resolution has been measured with both thick and thin vanadium targets. The energy resolution (FWHM) at .050 ev is 5.4%. At the same energy, the original design (assuming matched crystals and collimators) would have given a resolution of 7.6%. (The resolution varies as $\sqrt{E}$.)

(6) Signal and Background Intensities: The total count rate for 30° scattering from a polyethylene target of thickness equivalent to 83.5% transmission is 7.0 counts per minute at .05 ev. This is equivalent to a total count rate of about 5.0 counts per minute for 45° scattering from a 90% transmission water target at the reactor maxwellian peak. Of this the background count is approximately 0.9 counts per minute. These levels will soon be raised by a factor of two, when the power level of the Ford Nuclear Reactor is raised from 1.0 to 2.0 MW. Hence the minimum acceptable signal and background levels noted in the first Progress Report (10.0 and 2.0 counts per minute respectively) have been reached almost exactly. The low background level has been achieved by means of detector shielding which exceeds the cantilevered load capacity of the third arm. Hence, the use of a floor-supported wheeling carriage to support the detector shielding has become necessary.

(7) Experimental Scattering Data on C_nH_{2n} and H_2O: The scattering of .050 ev neutrons as a function of energy, angle, and temperature in polyethylene (C_nH_{2n}) has been started. The initial data, including angular distributions and an energy distribution at fixed scattering angle, are presented in Section E of this report. The energy distributions have sufficient resolution to indicate low-intensity energy transfers at 0.01 and 0.02 and possibly at 0.006 ev. These data will be published when they are supported by additional reruns. Upscattering data from water at 300°K and at a scattering angle of 70° show interesting energy peaks which may be interpreted as due to hindered transitional molecular motions. It is not yet clear whether these data conflict with the data from Chalk River. The results of the water data will probably be extended and reported in the near future.

C. CONSTRUCTION OF THE CRYSTAL SPECTROMETER

SHIELDING AND BACKGROUND LEVELS

As shown in Figs. 1 and 2, primary beam shielding is provided by a high-density masonite turret which can be rotated 30°. The direct γ and neutron beam is stopped by 6 in. of Pb and 30 in. of masonite. The direct beam profile as seen through a "straight on" port is shown in Fig. 3. The γ dose at this position is $\approx$ 300 r/hr with the port open and $\approx$ 2 mr/hr with the port closed. Fast and thermal neutron levels as seen by a survey meter directly in front of the closed port are 1.4 and 10 neutrons/cm^2/sec respectively. Portable 8 in. water tanks are being installed in front of the central section of the turret to further reduce fast neutron leakage. (These tanks must be moved to make room for extreme main-arm positions.)

A substantial background contribution occurs from side-scattered neutrons which escape from behind the turret. Originally, a deformable plastic water bag was installed to provide continuity of side-shielding. The bag proved impracticable because of possible water leakage, and has been replaced by a yoke of 7 tailored water tanks, visible in Fig. 2. The central section can be rolled forward on cantilevered tracks to permit access to the turret crystal well. Background levels are not significantly different for the bag and yoke arrangements, even at extreme turret positions.

External shielding along the scattering path is provided by borated paraffin cylinders formed so that they provide a continuous housing. The second Bragg collimator is surrounded by a 12-in. diameter shield, as is the Bragg detector. The second crystal well is an annulus 22 in. in diameter with a hole 10 in. in diameter. The turret port, analyzer crystal well, and 2-in.-diameter Bragg detector are lined with .030 in. of cadmium.

Extensive background level data show that for the Bragg detector:

a. the addition of the portable 8 in. turret water tanks reduced the background count by a factor of 2.1;

b. the addition of the 8 in. water yoke around the detector cylinder reduced the background by an additional factor of 2.0; and

c. the absolute background with this shielding is 0.9 counts per minute at one MW. (This value varies by about ±20%, depending on the position of the main arm.) (These data are for the RSN BF_3 tube described below.)

Because the detector yoke presents an additional cantilevered load of about 700 lb, it has become necessary to floor-support the detector arm. A support frame is now being installed; it is intended to run freely on large castered wheels bearing on a large, accurately leveled floor plate.

The detector shielding problem might be substantially improved by the use of large scintillation detectors instead of BF_3 tubes. This possibility is currently under investigation.

ANGULAR ROTATION METHODS

Accurately controlled and measured rotational motion about the three spectrometer axes is basic to the design. This motion includes (a) main-arm and turret rotation, which through a friction-held 2:1 linkage automatically tracks the first Bragg crystal; (b) scattering-arm rotation, which determines the target scattering angle; (c) target-table rotation; and (d) detector and second-crystal rotation.

The main arm is driven through a large, custom-made gear segment, visible in Fig. 4. This segment has one tooth per degree and is driven by a pinion with a reduction of 450. The over-all gear reduction to driving motor is 2250. This drive moves the main arm, turret, and first crystal; the motion can be directly read to 30 sec of arc, with vernier potential to 3 sec. As noted in the first Progress Report, the 2:1 tracking reliability accumulates 1 min of arc in a 90° arm rotation. Backlash in the total gear train is 1.9 min, and under the present adjustments seems to be constant.

The target table, scattering arm, and third crystal and detector are now operating with commercial stock gear elements. These generate random rotation errors of less than 1.0 min, due to imperfections in manufacturing or mounting. Blacklash is great enough to require uni-directional driving for all scanning runs. Vernier indicating accuracy is ±10 sec for all drives.

Provision has been made for a 2:1 band drive between the second crystal and the detector arm which is similar to the drive used for the first crystal. Because it has not yet been completed, only variable incident energy (E_0)—fixed scattering energy (E_S) experiments are feasible at present.

The main-arm, target, and scattering-arm gear trains are driven by three "Slo-Syn" d-c impulse motors requiring 200 power pulses per shaft rotation. Table I lists the total gear reduction and the required number of impulses per degree of arm or table movement.

Automatic scanning can simultaneously position these three drives in a non-linear program of motions if desired. Such a program is required for the scanning of inelastic scattering under either fixed-momentum or fixed-energy transfer. Figure 5 is a diagram of the monitor counting system; Fig. 6 is a

detailed version of the "Programmer" block in Fig. 5. The sequence is initiated by the output closure (start signal) from the monitor preset scaler. This signal starts an Eagle sequential timer, which first advances a punched card reader to a new position and then after a 2-sec delay resets all three motor pulse scalers (Beckman 7415 preset). The card reader sets the preset numbers on the scalers and also dictates the direction in which the drive motors rotate. (The direction can be reversed, depending on the starting relay configuration.) When the motor pulse scalers are reset, their output relays close and turn on motor pulsers which generate power pulses in the proper sequence and drive the motors. The pulses are counted by the scalers until the preset numbers are reached, at which time the output relays open, turning off the motor pulses. A relay "and" circuit generates a signal to reset the monitor scaler when all drives have stopped. The counting system begins at the new position immediately upon resetting the monitor scaler.

The programmer is partially complete at the present time. The motor pulser and the "and" relay circuits have been designed and built by us; the motor scalers have been ordered. A program card reader is being built by us to handle IBM punched cards. Meanwhile the system is operated manually.

When this scanning system is completed it should prove extremely simple and accurate. The impulse motors have an uncertainty in new shaft position of ±1.0 pulse, which corresponds to less than 5 sec of arc for any drive listed in Table II. If blacklash can be avoided, arbitrary advances of any drive should be positioned and reproducible to about ±10 sec of arc. This is more than sufficient for any liquid scattering experiment, and is probably also sufficient for crystal diffraction experiments.

DETECTORS

The detection system was outlined in the first Progress Report. The scattering detector is a commercial (Reuter-Stokes) BF_3 end-window proportional counter, 2 in. in diameter. The monitor is a pancake-shaped fission chamber which intercepts the entire E_0 beam at the exit of the turret port. The scattering detector channel is turned on and off by the accumulation of counts in the monitor channel.

The fission chamber is shown removed from its housing in Fig. 7 (which also shows the vernier-controlled Cd aperture at the turret exit). Figure 8 is a drawing of the chamber, showing dimensions. Because the monitor should have low sensitivity to gammas, low efficiency, and high transmission, the parallel-plate fission chamber is an ideal choice. The monitor is 1.0 in. thick, 5-1/2 in. in diameter, and has windows 3-1/2 in. in diameter. The windows consist of two 1100-S aluminum plates 0.050 in. thick, on which a deposit of 1 mg/cm^2 of 90%-enriched U^{235} has been deposited by electrolysis. These form the cathode; the anode is a 0.020 in. aluminum plate insulated by teflon spacers. The filling gas is 90% A—10% CH_4 at atmospheric pressure,

which in this chamber produces a rise time of the order of 2.0×10^{-7} sec. Count-rate responses to discriminator settings and high-voltage variations are shown in Fig. 9. The calculated absolute detection efficiency vs. energy is shown in Fig. 10. Typical counting statistics are 50,000 cpm at .05 ev. The detector operates as a pulse ionization chamber with high voltage set at 500 volts. The transmission is 97% and is essentially constant with energy, since the majority of neutrons are removed by scattering in the aluminum window. The monitor was designed and built as a Master's Degree project by a student at The University of Michigan.*

It should be noted that the accuracy of the calculated efficiency vs. energy is critical to the spectrometer system since with fixed scattering energy this is the only calculated correction to the observed intensities.

The scattering detector has a calculated absolute efficiency vs. energy shown in Fig. 11. This curve can be verified experimentally from the monitor response, if the monitor efficiency is assumed known. Because the BF_3 detector is so flat, an attempt was made to perform this verification in reverse order; the data points on Fig. 10 were made with the assumption that the calculation of Fig. 11 was correct. This cross-check will be refined by further work.

The detection system has been in successful operation for 5 months. Because both chambers must perform with the utmost reliability, weekend calibration checks are made by means of a portable Pu-Be neutron source. The accumulation time for the monitor is also checked against the reactor power level quoted by the operating personnel. But the monitor is the primary standard, and during a typical week of operation it has revealed reactor power drifts of the order of 6%. The monitor has exhibited excellent stability. The BF_3 detector is also very stable but insulation noise, apparently caused by leaks across the teflon HV connector insulation, has twice interrupted the program.

*E. Straker, "Design and Construction of a Parallel Plate Fission Chamber," unpublished Master's Thesis, Phoenix Memorial Laboratory, 1962.

D. CALIBRATION OF THE SPECTROMETER

MEASUREMENTS ON MONOCHROMATING CRYSTALS

The incident neutron energy is selected from the Maxwellian spectrum of the reactor-port leakage flux by Bragg reflection off the 200 planes of a 3 in. x 6-1/2 in. copper half-cylinder crystal. The orientation relative to the scattering directions is shown in Fig. 12. The scattered neutrons are energy-analyzed by a second (the other half-cylinder) copper crystal.*

In selecting the best crystals, both good resolution and good reflectivity are desired. For neutron absorption and scattering, these properties depend on several known parameters, such as the lattice constants, and on the microscopic cross-section for neutron absorption and scattering. One parameter upon which these properties depend, the crystal structure factor η as seen by neutrons, is not available in the literature. It is customarily assumed that the "mosaic blocks," the misorientation of sub-crystals about the nominal Bragg planes, obey a gaussian distribution

$$\omega(\epsilon)\,d\epsilon = \frac{1}{\eta\sqrt{2\pi}}\, e^{-\epsilon^2/2\eta^2}\, d\epsilon. \qquad (1)$$

Single or double "crystal rocking" experiments can be performed to infer η. If η is known, the reflectivity and resolution of a particular sample can be calculated, which makes selection of the optimum monochromator possible, in principle. This program will be followed in selecting a better monochromator, if possible. The copper crystals, however, were purchased before this program was well underway and may not be a best choice for our purposes, because the mosaic width is less than anticipated. Furthermore, our data, thus far taken show that η is only very crudely constant and exhibits much variation even in a single sample (see the NaCl data of Table II).

The experiment we have performed is an angular (θ) rocking of the crystal through its Bragg maximum when (a) the source flux is Maxwellian, (b) the source flux is angularly defined by an initial collimator, and (c) the Bragg scattered flux is angularly defined by a second collimator. All flux transmitted by the second collimator is intercepted by a BF_3 detector. Figure 13 shows the arrangement used.** The initial collimator is a slit of width s = 1/8 in. and length l = 48 in. The beam width at the crystal is 3/16 in. and the detector is located 54 in. from the crystal axis behind a 3/16 in. collimating slit. The sample crystal is mounted in a motor-

*Prepared by Semi-Elements, Inc., Saxonburg, Pennsylvania.

**Measurements were made at the student spectrometer facility of the Ford Reactor.

driven carriage that turns at a constant speed of 14.85 min/min. Optimization of tilt about a horizontal axis is provided, as is horizontal translation for scanning crystal faces over a 1 in. range. As the crystal is turned, the counting rates are traced on a strip-chart recorder.

These measurements can be interpreted under the reasonable assumptions that (a) the source is isotropic and slowly varying in energy (i.e., a "white" spectrum) and that no order contamination exists, and (b) the transmission probabilities of crystal and collimators are all gaussian. Under these assumptions the observed count rate can be given by

$$CR(\theta,\alpha_o) = \iint \Phi(\phi,\theta_o) P_1(\phi) P_x(\epsilon) P_2(\alpha-\alpha_o)\, d\theta_o d\phi \qquad (2)$$

where the angles, shown in Fig. 14, are

ϕ = angle at which neutrons leave the first collimator, measured from the collimator axis

θ = angle between first collimator axis and the nominal Bragg planes

α = Bragg scattering angle

α_o = angle between the two collimator axes

ϵ = misorientation angle between particular mosaic planes and nominal Bragg planes

θ_o = angle that satisfies the Bragg condition for a particular incident wavelength and a particular mosaic element

and where the collimator transmission probabilities are

$$P_1(\phi) = C_1 e^{-\phi^2/2\sigma_1^2}$$

$$P_2(\alpha-\alpha_o) = C_2 e^{-(\alpha-\alpha_o)^2/2\sigma_2^2} \qquad (3)$$

and the crystal transmission probability is

$$P_x(\epsilon) = \frac{\mathcal{R}}{\sqrt{2\pi}\,\beta} e^{-\epsilon^2/2\beta^2}. \qquad (4)$$

The source flux is $\Phi(\phi,\theta_o)$ given in neutrons per unit collimator angle per unit Bragg angle. Geometrically, the collimators have a triangular distribution with full widths at half maximum (FWHM) W_{C_1}, W_{C_2} equal to the slit width-to-length ratios $(s/\ell)_1$, $(s/\ell)_2$. In the gaussian representation, we assume the same half widths, so that σ_1, σ_2 are defined by

$$W_{C_{1,2}}^2 = \left(\frac{s}{\ell}\right)_{1,2}^2 = 8\ell n2\ \sigma_{1,2}^2 \tag{5}$$

C_1, C_2 are constants. The assumed crystal width is

$$W_x^2 = 8\ell n2\ \beta^2$$

and $\mathcal{R}$ is the true integrated reflectivity. The actual crystal transmission is a "flattened" gaussian given by the unintegrated reflectivity function (reflection case with absorption)

$$R(\epsilon)d\epsilon = \frac{a\,d\epsilon}{(1+a) + \sqrt{1+2a}\ \coth\ (A\sqrt{1+2A})} \tag{6}$$

where

$$a = \frac{Q}{\mu}\ \frac{1}{\sqrt{2\pi}\ \eta}\ e^{-\epsilon^2/2\eta^2}, \qquad A = \frac{t_o\mu}{\cos\ \gamma}$$

in which μ, t_o, γ, and Q are, respectively, the microscopic "linear" absorption coefficient,* the thickness of the crystal, the angle of incidence relative to the crystal face, and the sub-crystal reflectivity.** $\mathcal{R}$ is the integral of Eq. (6), and for practical cases β is between 1.0 and 2.0 x η.

The angles Θ, α_o are parameters of the experiment; θ_o is a variable of the source energy. From Fig. 14 it is seen that α, β can be represented as dependent variables

$$\begin{aligned} \alpha &= \phi + 2\theta_o \\ \epsilon &= \theta_o - \Theta + \phi \end{aligned} \tag{7}$$

*Contrary to certain usage, μ is proportional not to the total cross-section but to the total cross-section minus the coherent scattering cross-section, i.e., $\mu = N(\sigma_t - \sigma_{s_{coh}})$.

**G. Bacon, Neutron Diffraction, Oxford University Press, 1962, p. 69.

Hence, Eq. (2) can be written as a double convolution

$$CR(\Theta,\alpha_o) = \frac{C_1 C_2 \mathcal{R}(\bar{\Theta}_o)\Phi(\bar{\Theta}_o)}{\sqrt{2\pi}\,\beta} \iint_{-\infty}^{+\infty} e^{-\frac{\phi^2}{2\sigma_1^2}} \cdot e^{-\frac{(\Theta_o-\Theta+\phi)^2}{2\beta^2}} \cdot e^{-\frac{(\phi+2\Theta_o-\alpha_o)^2}{2\sigma_2^2}} d\phi d\Theta_o \tag{8}$$

whose solution is

$$CR(\Theta,\alpha_o) = \frac{K\mathcal{R}(\bar{\Theta}_o)\Phi(\bar{\Theta}_o)}{\sqrt{\sigma_1^2+\sigma_2^2+4\beta^2}}\; e^{-(\frac{\alpha_o}{2}-\Theta)^2/(2\beta^2+\frac{\sigma_1^2+\sigma_2^2}{2})} \tag{9}$$

If α_o is held constant this selects an optimum count rate corresponding to the energy for which $\Theta_o = \alpha_o/2$ and a gaussian is generated by rocking Θ. The total width is

$$W^2 = 8\ell n2(\beta^2 + \frac{1}{4}\sigma_1^2 + \frac{1}{4}\sigma_2^2) \tag{10}$$

or

$$W_x^2 = W^2 - C$$

where C is a system constant.

From Eq. (10), β can be obtained and η calculated by comparison of Eqs. (4) and (6). Figure 15 is a calculation of β vs. η for several crystals. Finally, $\mathcal{R}$ is calculated from this choice of η. C can be calculated (giving 55.5 square minutes in this experiment), but is best found by measuring W for a test crystal such as calcite for which $W_x \ll W$. For lack of calcite we have used our narrowest NaCl data, which gives $W^2 = 43.5 \pm 6.5$ square minutes as a close approximation to C.*

Table II lists measurements made on samples thus far obtained. All curves were taken at a mean wavelength of $\sqrt{2}$ Å. The Be crystal was obtained from Nuclear Metals, Inc.; the Cu and Zn crystals were obtained from Semi-Elements. The Pb and NaCl were originally obtained from Argonne National Laboratory, but have an uncertain history. The Al crystal represented a first attempt in this laboratory to grow large crystals and showed multiple crystal structure. It is believed that as yet only the Be, Cu, and Zn data are trustworthy. Additional Pb crystals are being procured and the growth of 3 in.-diameter Zn and Al crystals is in progress. Typical rocking curves are shown in Figs. 16 and 17.

*Subsequently, we obtained a calcite crystal but found that it gives a poor response in the absence of fresh cleavage faces.

Reflectivities ($\mathcal{R}$) were calculated for these crystals vs. η and are shown in Fig. 18. The solid data points correspond to the measured η. If these results are assumed to be correct, one must conclude that the choice of Cu is not particularly attractive with regard to intensity but is excellent with regard to resolution. The Cu monochromators were purchased under the assumption (gleaned from published data on Cu-111 planes) that the η was about 4 min.

The analysis from Eq. (2) is an approximation in that the spatial position of neutron rays is ignored. For some experiments, a space-angle correlation exists such that transmission functions are not simple gaussians. This is the case for the present experiment but is not the case for the analysis of Energy Resolution below (because the scattering target effectively removes the space-single correlation). Exact expressions are being studied and will probably require machine computation. Measurements on numerous crystals are also in progress. From an economic viewpoint home-growing of crystals appears to be most practical. Because intensity is a major problem, this effort is felt to be worthwhile.

ENERGY RESOLUTION

The spread in energy about E_o for incident neutrons hitting the scattering target is determined by the source collimator and first crystal monochromator. The uncertainty in scattered energy about E_s is likewise determined by the second collimator and second monochromating crystal. The collimators following each crystal are for shielding only and are not intended to be limiting in angle. (It can be easily shown, in fact, that additional resolving collimation should be avoided where multiple slit collimation is used; the total flux is greatly reduced with no appreciable improvement in resolution.*)

A general expression for the observed count rate due to scattering from any target can be written from an elaboration of Eq. (2). For the triple-axis system of Fig. 19 the detected count rate will have the form

*This is best displayed by the graphical scheme proposed by J. Carpenter, "A Construction for the Investigation of Collimator Performance," to be published.

$$CR(\theta_1,\theta_2,\alpha_o) = \int\cdots\int \Phi(\theta_o,\phi_1)P_1(\phi_1)\delta(\phi_1+\theta_1-\theta_o-\epsilon_1)P_{X_1}(\epsilon_1)P_t(\alpha_o-\phi_2,\theta_o,\theta_f)P_2(\phi_2)$$
$$\times\ \delta(\phi_2+\theta_2-\theta_f-\epsilon_2)P_{X_2}(\epsilon_2)\mathcal{E}(\theta_f)\,d\theta_o d\phi_1 d\epsilon_1 d\theta_f d\phi_2 d\epsilon_2 \qquad (11)$$

where the delta functions express the restrictions on ϵ_1, ϵ_2 imposed by the Bragg reflections; and where θ_1, θ_2 and α_o are parameters of the experiment, being respectively the incident and exit Bragg crystal settings and the mean scattering angle. $\Phi(\theta_o,\phi_1)$ is the source flux impinging on the first collimator per unit Bragg angle (energy) and per unit collimator angle in the scattering plane. $P_1(\phi_1)$ and $P_2(\phi_2)$ are, as before, the collimator transmission probabilities per unit angle of incidence in the scattering plane from an extended source. $P_{X_1}(\epsilon_1)$ and $P_{X_2}(\epsilon_2)$ are the crystal transmission probabilities. $P_t(\alpha_o-\phi_2,\theta_o,\theta_f)$ is the target scattering probability. This probability is proportional to the differential scattering cross-section $\sigma(\Omega,\theta_o,\theta_f)$ and is the fraction of neutrons incident on the target which, after scattering, enter the detector collimator. $\mathcal{E}(\theta_f)$ is the efficiency of the detector at the scattered energy corresponding to θ_f.

If we examine the simplest experiment--namely, scattering from a target whose cross-section is purely elastic, incoherent, and isotropic—Eq. (11) becomes quite simple, particularly since the scattering angle is independent of the incident conditions. Since under these conditions $E_o = E_f$, $P_t(\alpha_o-\phi_2, \theta_o,\theta_f) \approx P_t(\alpha_o,\bar{\theta}_o)$ and since the source flux is slowly varying in energy (θ_o) and is constant in ϕ_1, we write

$$CR(\theta_1,\theta_2,\alpha_o) \approx \Phi(\bar{\theta}_o)P_t(\alpha_o,\bar{\theta}_o)\mathcal{E}(\bar{\theta}_o) \qquad (12)$$
$$\iiint P_1(\phi_1)P_{X_1}(\phi_1+\theta_1-\theta_o)P_2(\phi_2)P_{X_2}(\phi_2+\theta_2-\theta_o)\,d\phi_1 d\phi_2 d\theta_o$$

For these scattering conditions, the absolute value of each term in Eq. (12) can be stated as follows:

$$\Phi(\bar{\theta}_o) = I_o\left(\frac{s_1 h_1 n_1}{2\pi}\right)\tilde{\Phi}(\bar{\theta}_o)$$

where

I_o = source flux intensity in neutrons/cm^2/sec measured at the source collimator entrance for an <u>infinitely extended</u> source plane

$\tilde{\Phi}(\bar{\theta}_o)$ = normalized Maxwellian distribution function per unit Bragg angle, i.e.,

$$\tilde{\Phi}(\bar{\theta}_o) = \frac{2E_o^2}{(kt)^2} \cot \bar{\theta}_o \, e^{-E_o/kt}$$

and s_1, h_1, n_1 = source collimator slit width, height, and number respectively.

$$P_t(\alpha_o,\bar{\theta}_o) = \frac{(1-t[\bar{\theta}_o,\alpha_o])}{2A_1} \left(\frac{s_2 h_2 n_2}{2\pi}\right)$$

where

$(1-t)$ = fraction of incident neutrons scattered in a thin target

A_1 = effective area of the beam incident on the target

and s_2, h_2, n_2 describe the second collimator.

$$P_{1,2}(\phi_{1,2}) = \sqrt{4\ell n2/\pi} \left(\frac{h}{\ell}\right)_{1,2} e^{-\phi_{1,2}^2/2\sigma_{1,2}^2}$$

and for identical crystals, we have, as before,

$$P_{x_{1,2}}(\epsilon_{1,2}) = \frac{\mathcal{R}(\bar{\theta}_o)}{\sqrt{2\pi}\,\beta} e^{-\epsilon_{1,2}^2/2\beta^2} .$$

The integrals over ϕ_1, ϕ_2 and θ_o yield,* finally

$$CR(\theta_1,\theta_2,\alpha_o) = K(\bar{\theta}_o,\alpha_o) \, e^{-(\theta_1-\theta_2)^2/2\gamma^2} \qquad (13)$$

where

$$\gamma^2 = (2\beta^2+\sigma_1^2+\sigma_2^2) = \frac{(2W_x^2+W_{C_1}^2+W_{C_2}^2)}{8\ell n2}$$

*The integration over ϕ_1, ϕ_2 only yields

$$\frac{d(CR)}{d\theta_o} = K \cdot \left(\frac{2(\beta^2+\sigma_1^2+\sigma_2^2)}{2\pi(\beta^2+\sigma_1^2)(\beta^2+\sigma_2^2)}\right)^{1/2} \cdot e^{-\left(\frac{[\theta_1-\theta_o]^2}{2[\beta^2+\sigma_1^2]} + \frac{[\theta_2-\theta_o]^2}{2[\beta^2+\sigma_2^2]}\right)} .$$

If, for simplicity, we put $\theta_1 = \theta_2$, $\sigma_1 = \sigma_2$, we see that the energy content of the detected beam is gaussian with a FWHM of $W = 2\sqrt{\ell n2}\,(\beta^2+\sigma^2)^{1/2}$, which is smaller by $\sqrt{2}$ than the incident energy width.

and

$$K(\bar{\theta}_o,\alpha_o) = \frac{I_o \mathfrak{F}(\bar{\theta}_o)\,\mathcal{E}(\bar{\theta}_o)\,\mathcal{R}(\bar{\theta}_o)^2}{\sqrt{2\pi}\,(2\beta^2+\sigma_1{}^2+\sigma_2{}^2)^{1/2}} \cdot (1-t[\bar{\theta}_o,\alpha_o])(s_1h_1n_1)\left(\frac{s_2h_2n_2}{2A_1}\right)\left(\frac{\Omega_1}{2\pi}\right)\left(\frac{\Omega_2}{2\pi}\right) .$$

Equation (13) expresses the apparent angular (and hence energy) uncertainty observed by the spectrometer when the scatterer is a delta function in energy and is "constant" in angle at least over the spectrometer aperture. The FWHM of the distribution, as θ_1 is varied relative to θ_2, is $(2W_x{}^2+W_{C_1}{}^2+W_{C_2}{}^2)^{1/2}$, which is independent of $\bar{\theta}_o$. The respective widths for our system are 8.8 min, 25.6 min, and 27.7 min; hence we should expect a constant rocking curve of 39.7 min.

Figures 20 and 21 show rocking curves measured at .030, .050, .063, and .080 ev with a vanadium target used for which 1-t was approximately 0.19 for the 0.246-in. thickness, and 0.10 for the 0.123-in. thickness. The curves for the thinner vanadium target demonstrate the insensitivity of elastic events to multiple scattering effects. Figure 22a is a plot of the angular width W vs. energy or Bragg angle compared with the expected constant result from Eq. (13). Finally, Fig. 22b is a plot of the apparent energy resolution vs. energy, R(E) = W 2cot $\bar{\theta}_o$.

It appears from these results that the spectrometer resolution is well predicted by simple theory, although the observed resolution is about 12% smaller than calculated.

INTENSITY MEASUREMENTS

As repeatedly noted, the primary difficulty with the spectrometer is lack of source intensity. In order to anticipate the extent of this difficulty and the possibility of improvements, the expected count rate was calculated and can be compared with present observations.

The calculated intensity is given by the amplitude, $K(\theta_1 = \theta_2)$ of Eq. (13), multiplied by the ratio of detector area to approximate beam area at the detector. Beam areas both at the detector and target positions were measured by neutron photographs.* Detector efficiency, collimator transmission, and $(\bar{\theta}_o)$ were calculated. Activation measurements of I_o were made at low power at the reactor source end of the port plug. The following values were found for 0.04 ev:

*A modified polaroid camera equipped with a Li-B-ZnS film backstop was kindly supplied by Dr. A. Arrott of the Ford Scientific Laboratory.

$$I_o = 2.2 \times 10^{12} \text{ neutron/cm}^2\text{/sec}$$

$$\Phi(.04) = 2.06$$

$$\mathcal{E}(.04) = 0.72$$

$$1\text{-}t = 0.16^*$$

$$\mathcal{R}(.04) = 2.4 \times 10^{-3}$$

$$s_1, h_1, n_1 = 0.358 \text{ in.}, 0.80 \text{ in.}, 3$$

$$s_2, h_2, n_2 = 0.194 \text{ in.}, 2.00 \text{ in.}, 9$$

$$\Omega_1/2\pi = s_1 h_1 / \ell_1^2 2\pi = 1.98 \times 10^{-5}$$

$$\Omega_2/2\pi = s_2 h_2 / \ell_2^2 2\pi = 1.07 \times 10^{-4}$$

$$\beta = 3.7 \text{ min}$$

$$\sigma_1 = \frac{s_1}{\ell_1} \frac{1}{2\sqrt{2\ell n 2}} = 10.8 \text{ min}$$

$$\sigma_2 = \frac{s_2}{\ell_2} \frac{1}{2\sqrt{2\ell n 2}} = 11.7 \text{ min}$$

$$A_1 = 5.90 \text{ in.}^2$$

$$A_2 = 10.3 \text{ in.}^2$$

$$A_o = 3.14 \text{ in.}^2$$

This gives for $\frac{A_o}{A_2} \times K(\theta_1 = \theta_2)$ a count rate of 15.1 cpm for the vanadium peak. Air scattering at reasonable humidity should reduce this value to 12.2 cpm. The observed value is 5.5 cpm. The agreement is within the uncertainties of the many parameters used.

To verify the calculation, the more directly obtained intensity at the monitor position was calculated and measured. The calculated intensity, a simple version of Eq. (13), is given by

$$CR(\bar{\theta}_o) = I_o \, \Phi(\bar{\theta}_o) \, \frac{\Omega_1}{2\pi} \, n_1 \mathcal{R}(\bar{\theta}_o) \mathcal{E}(\bar{\theta}_o).$$

*Because of vanadium absorption this is (1-t) = .19, due to scattering reduced by the absorption loss.

This gives a value of 1,100 cps. Air scattering should reduce this number to 950 cps, which is in close agreement with the observed value of 815 cps.

These results reveal several improvements within practical reach: increase in Bragg detector area, removal of air scattering, and optimization of core leakage flux. At 2.0 MW operation an intensity of 25 cpm should be well within realizable bounds, but at the expense of increased background, of course.

E. INITIAL SCATTERING EXPERIMENTS ON C_nH_{2n} AND H_2O

MEASUREMENTS ON C_nH_{2n}

Energy-integrated angular differential scattering and fixed-angle energy differential scattering have been observed for room-temperature polyethylene (C_nH_{2n}) in the initial part of a temperature-dependent polyethylene scattering cross-section program. These scattering data are shown in Figs. 23 and 24.

The angular data were gathered partly to determine if a simple correction for target thickness were the only correction required for angular distribution data. The corrected data were therefore normalized at 30° to similar data taken by Whittemore and McReynolds.* In both cases, the observed count rate is an energy integral as produced by a "flat" BF_3 counter with a response similar to that shown in Fig. 11. In Fig. 23 the abscissa $Q_o = \frac{4\pi}{\lambda_o} \sin \frac{\Phi}{2}$ is the momentum transfer as a function of laboratory scattering angle, if the scattering is assumed to be primarily "elastic" about the wavelength λ_o. In this case the plot should be independent of E_o. Within the accuracy of the data and equivalence of counters, no discrepancy occurs between the Whittemore data (large points) and the present data (small points). (The triangles in Fig. 23 correspond to a considerably different incident energy). It is interesting to observe the closeness of fit to a gaussian, $e^{-(Q_o u)^2}$, where u is close to the value 0.108Å. Such response can be interpreted as representing the Debye-Waller factor for polyethylene.**

Some inelastic scattering data from room temperature polyethylene is shown in Fig. 24. These data were obtained at 30° scattering angle for a fixed E_s = 0.05 ev and E_o scanned from .026 to .095 ev. The data represent three successive scans. The dashed curve superimposed on the elastic peak is the resolution function measured with a V target and was obtained, point for point, by alternating the V with C_nH_{2n} targets. The following observations can be noted about these data:

a. No diffusive broadening is evident in the elastic peak at room temperature (300°K).

---

*Whittemore, W. L., and McReynolds, A. W., "Inelastic Scattering of Thermal Neutrons Produced by an Electron Accelerator," Proceedings of the Symposium on Inelastic Scattering of Neutrons in Solids and Liquids, Vienna, 11-14 October 1960.

**Brockhouse, "Structural Dynamics of Water by Neutron Spectrometry," Neuvo Cimento, Supplement to Vol. IX, Series X, 1958, p. 45; Singwi and Sjolander, PR, 119, 866, 1960.

b. There is strong evidence of the existence of up-scattered energy transfers at $\Delta E \approx +.01$, $+.02$ ev and down scatter at $\Delta E \approx -.01$, $-.02$, $-.03$ ev. There is also indication of energy transfers at $\pm.006$ ev. However, the structure is not well defined. This may be due to angle jitter in our system, not as yet understood, since the scatter of points seems to be greater than warranted by statistics. None of these peaks have been reported from infrared spectroscopy.* The intensity of all the peaks is quite low.

c. There is some evidence of a very slight shift in the elastic peak. The shift amounts to +0.003 ev and is presumably caused by target recoil for poly relative to V.

d. The data shown in Fig. 24 represent 75 hours of reactor running time. The data at the subsidiary peaks have about 20% statistics and were made at a total count-to-background ratio of about 1.8.

MEASUREMENTS ON H_2O

Some measurements have been attempted on H_2O primarily for comparison with data at other sites, but also because of current interest at the University in the existence of crystal-like hindered translational levels spaced about the elastic peak.**

Figure 25 is a plot of angular cross-section data due, as before, to "flat" counter energy integration. Our data compare quite closely with the Brockhouse data,*** although ours more closely follow the gaussian $e^{-(Q_0 u)^2}$ suggested by Brockhouse.

Figure 26 shows inelastic data taken for a scattering angle of 70°, $E_s = .055$ ev and variable E_0. The appearance of satellite peaks is attributed to regularly spaced, hindered translational energy transfers. Preliminary attempts to match these peaks with a calculational model are underway. If the data can be firmly reproduced, they will be published shortly.

---

*Krimm, S., "Infra-Red Spectra of High Polymers," Fortschritte der Hochpolymeren-Forschung, Springer Verlag, Berlin, 1960.

**S. Yip, "The Scattering of Slow Neutrons by Polar Liquids," unpublished thesis, The University of Michigan, 1962.

***Brockhouse, op. cit., p. 18.

TABLE I

ROTATIONAL MOTION FROM MOTOR DRIVES

Component	Total Gear Reduction	Motor Impulses/ Degree of Motion
Main Arm	2250	1250
Scattering Arm	1440	800
Target Table	1600	888

TABLE II

SUMMARY OF CRYSTAL ROCKING DATA

Crystal Plane	Observed Width, W ($\lambda = \sqrt{2}$ Å)	Crystal Width, W_x	η	Peak Counting Rate	μ	Calculated Reflectivity [$R(\theta_o)$]	Values From the Literature	Reference
Be-0002	17.6' ± 6.6%	16.3' ± 9%	3.2'	4.16	.000933	.00440	η = 5.16'	Holm 100-16115
Cu-200	10.9' ± 9.6%	8.7' ± 19%	1.9'	2.22	.247	.00210	$W_x \simeq$ 20'	Weiss PR 83
NaCl-200	6.6' ± 7.6%	---	---	1.00	---	---	W_x = 8' η = 4'	Pasternack PR 81 Holm 100-16115
NaCl-200	15.3' ± 8.4%	13.8' ± 12%	---	0.47	---	---	---	---
Zn-0002	14.9' ± 3.5%	13.4' ± 6%	3.7'	---	---	---	---	---
Zn-0002	16.2' ± 5.3%	14.8' ± 8%	4.2'	3.20	.0562	.00265	---	---
Zn-0002	17.0' ± 5.3%	15.7' ± 8%	4.5'	---	---	---	---	---
Al-200	12.0'	10.0'	2.3'	1.51	.0107	.00260	---	---
Pb-200	49.4' ± 18.7%	48.9' ± 19.2%	---	1.39	---	---	---	---
Pb-200	18.6' ± 6.7%	17.4' ± 7.5%	4.3'	0.68	.00437	.00435	---	---
Pb-111	---	---	---	---	---	---	W_x = 20'	Pasternack PR 81

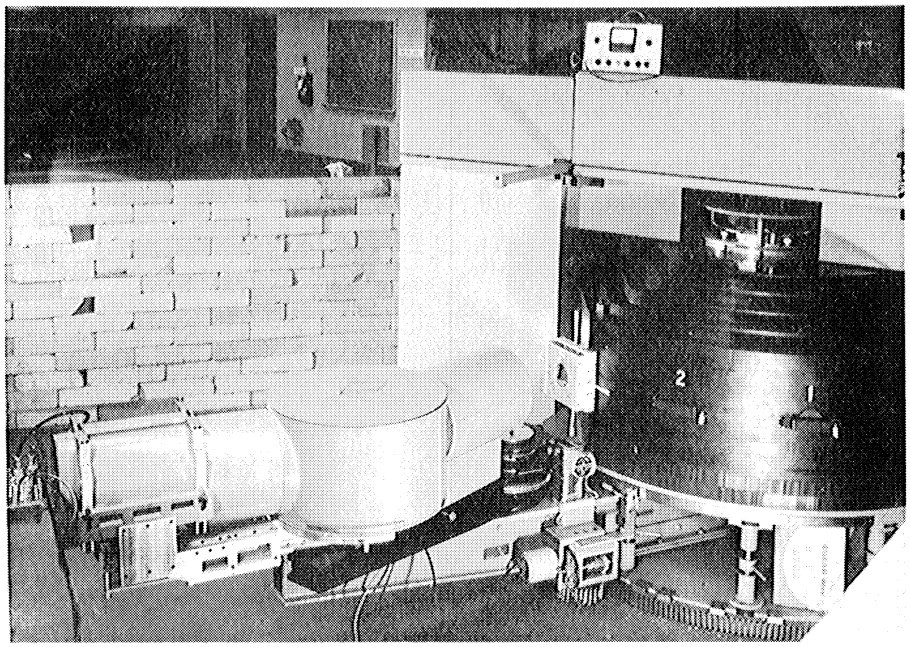

Fig. 1. Triple-axis spectrometer.

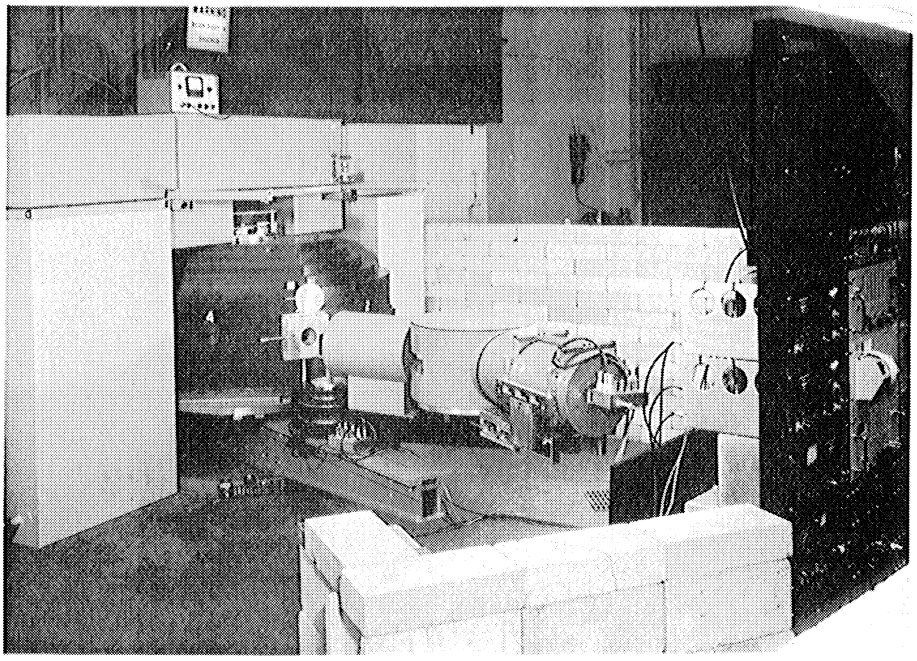

Fig. 2. Spectrometer showing shielding yoke.

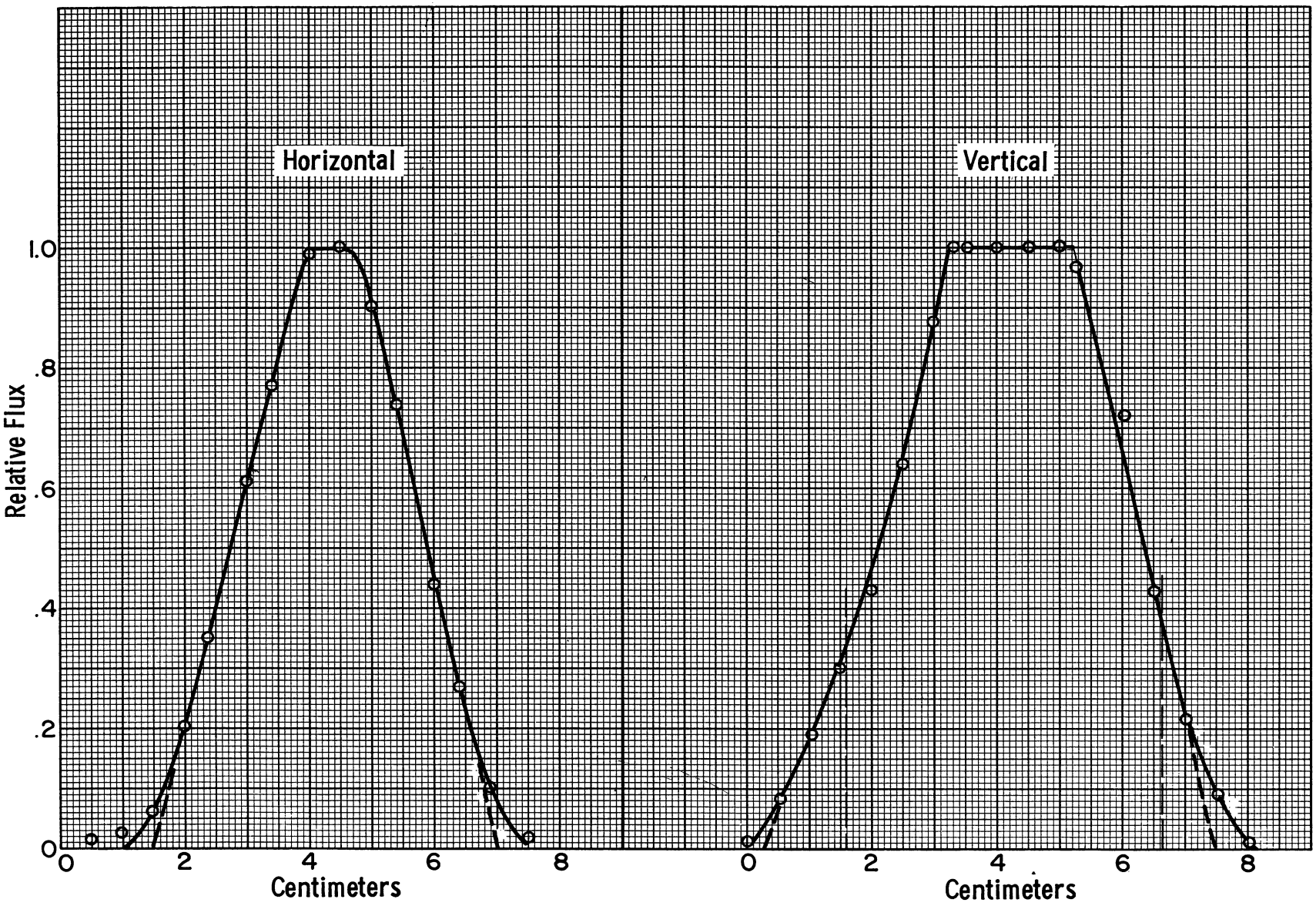

Fig. 3. Direct beam profile at turret exit.

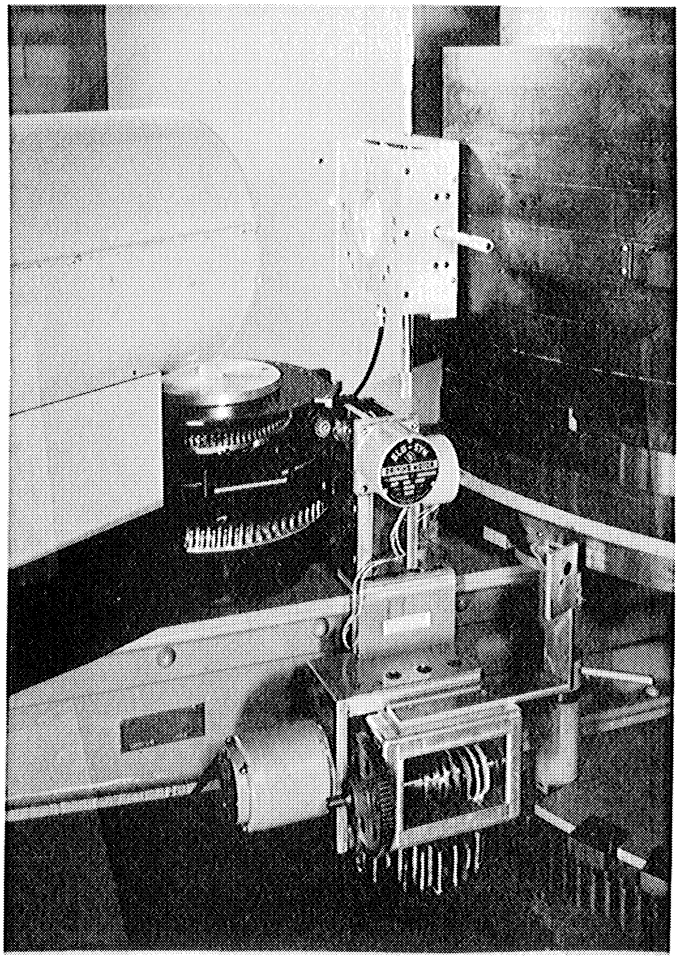

Fig. 4. Driving gear assemblies.

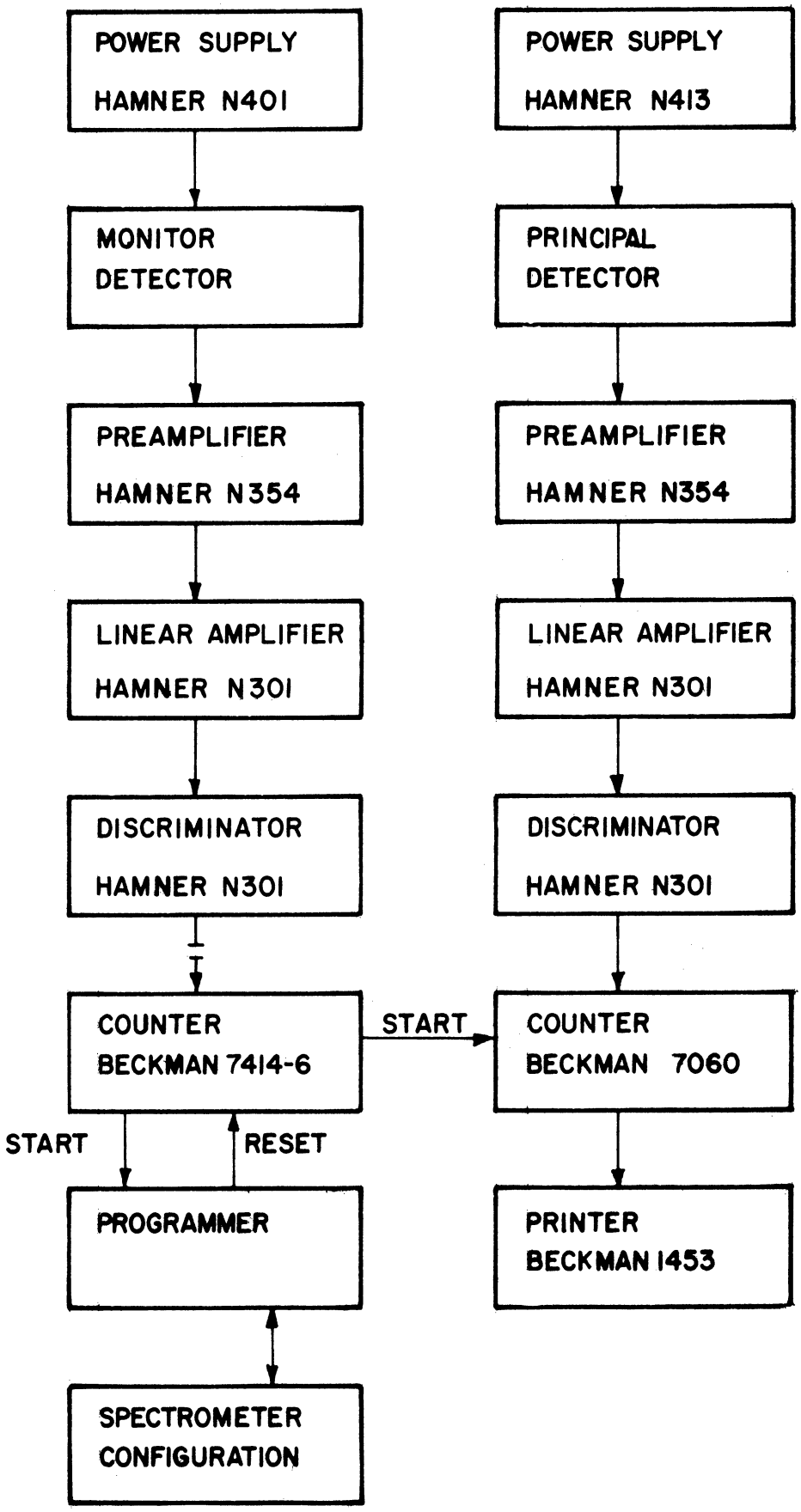

Fig. 5. Counting system.

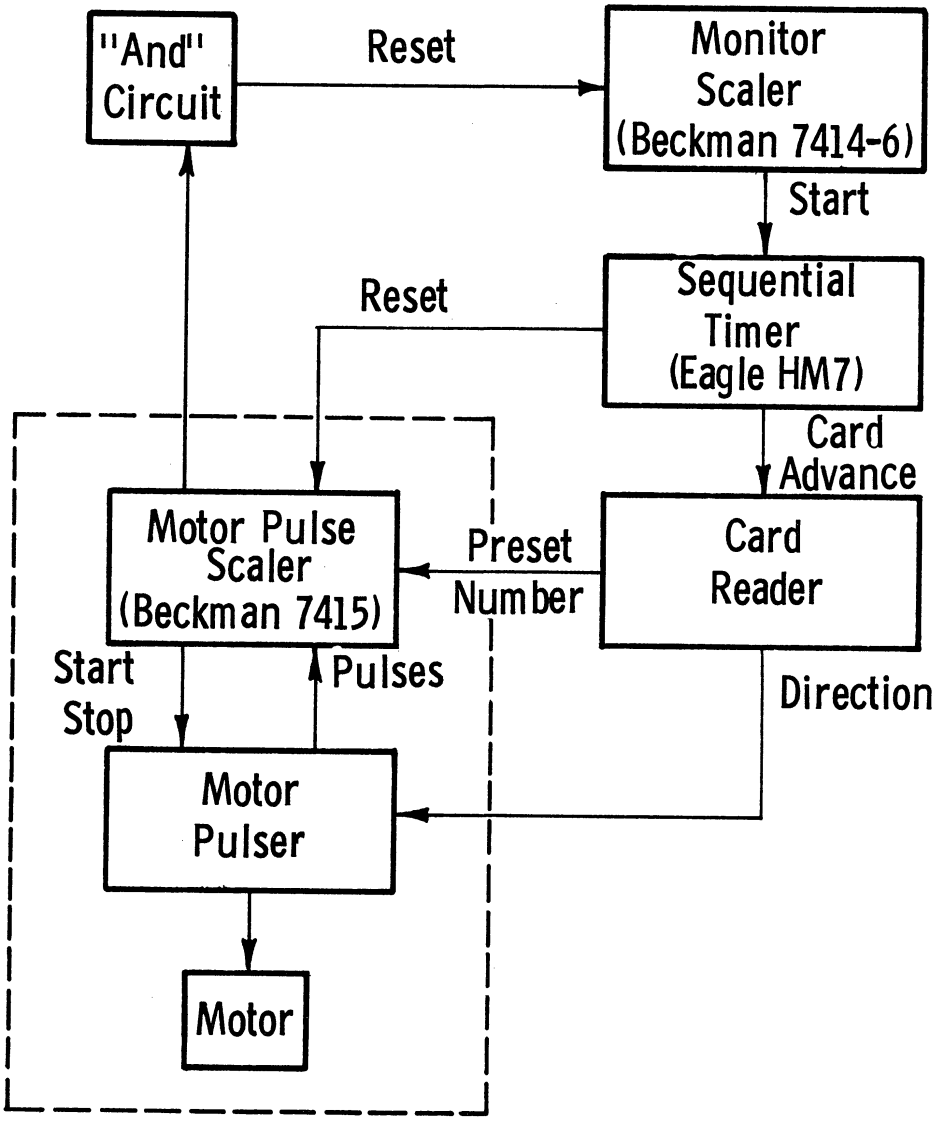

Fig. 6. Programmer schematic.

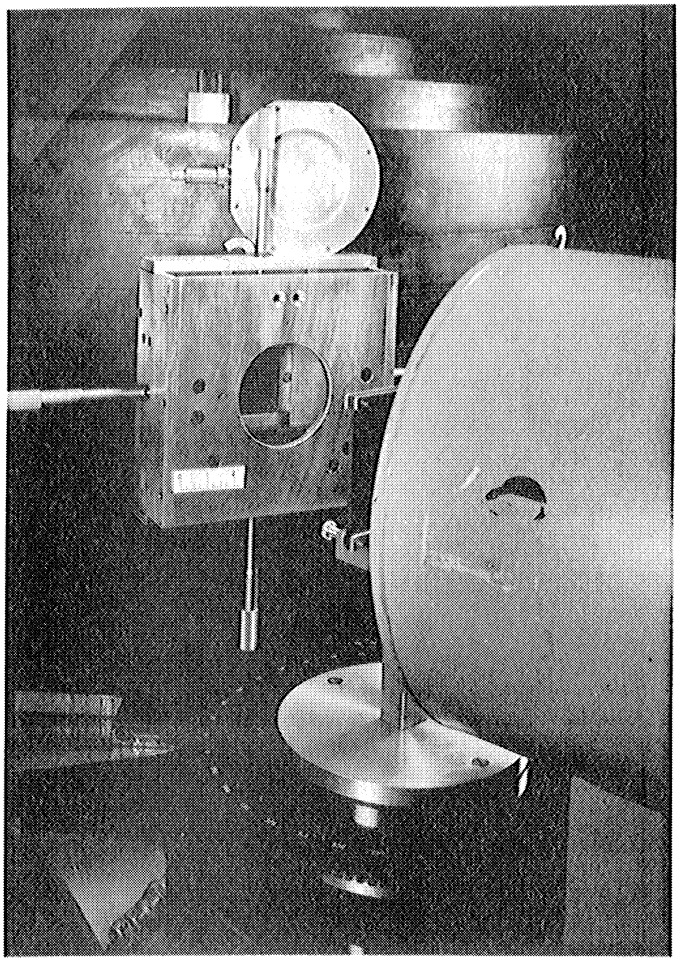

Fig. 7. Monitor and monitor housing.

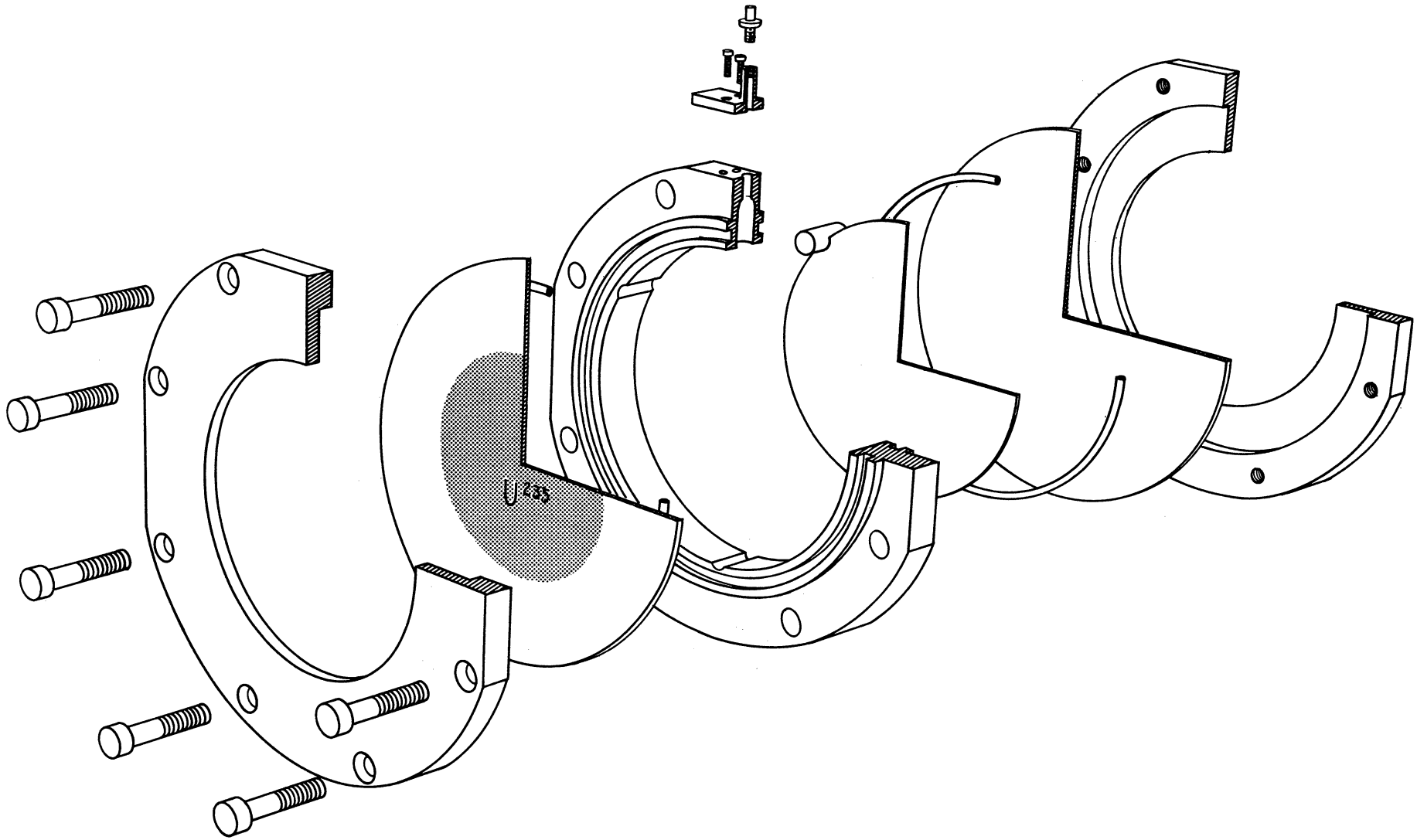

Fig. 8 Monitor design—parallel plate fission chamber.

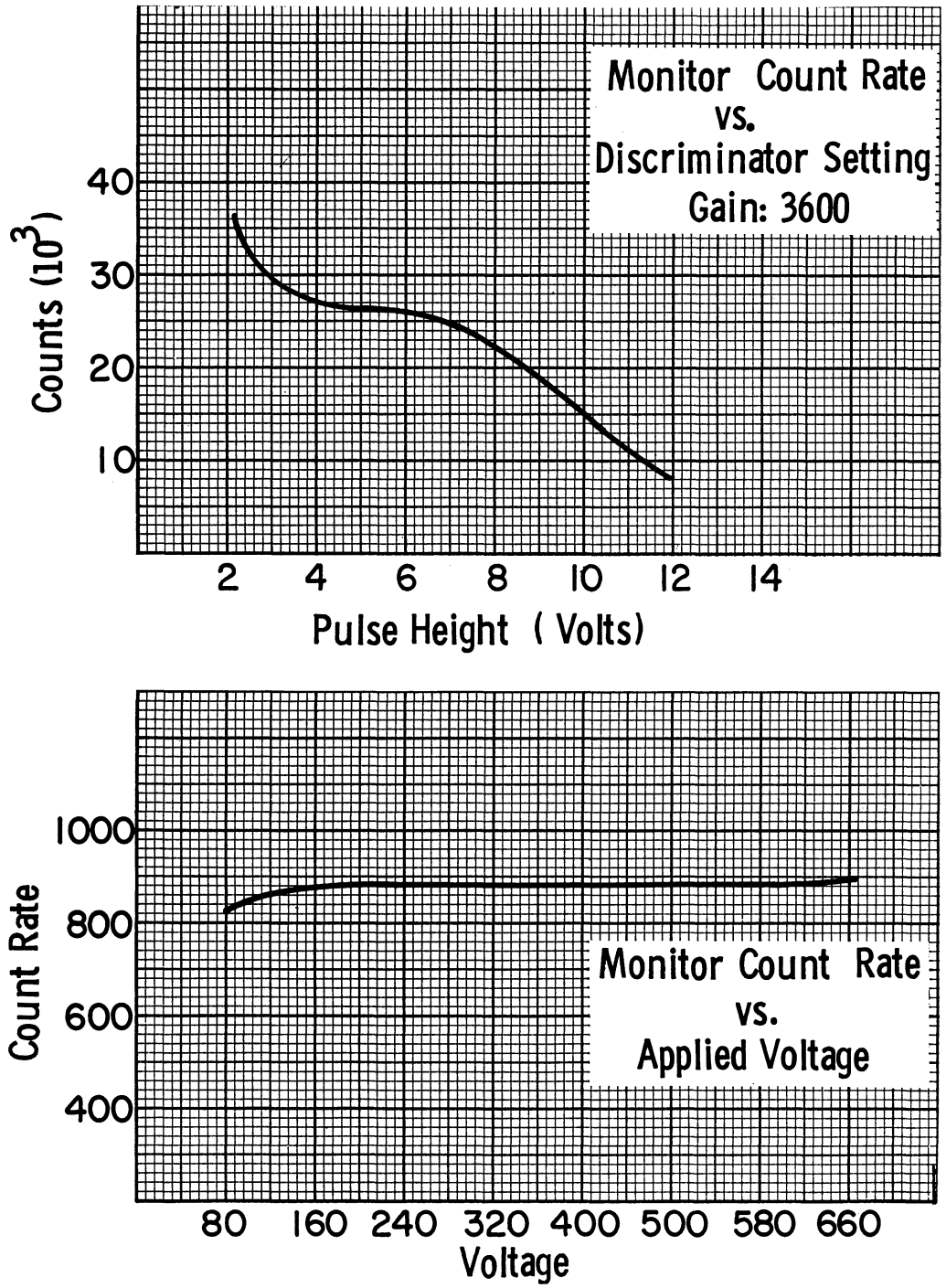

Fig. 9. Monitor counting characteristics.

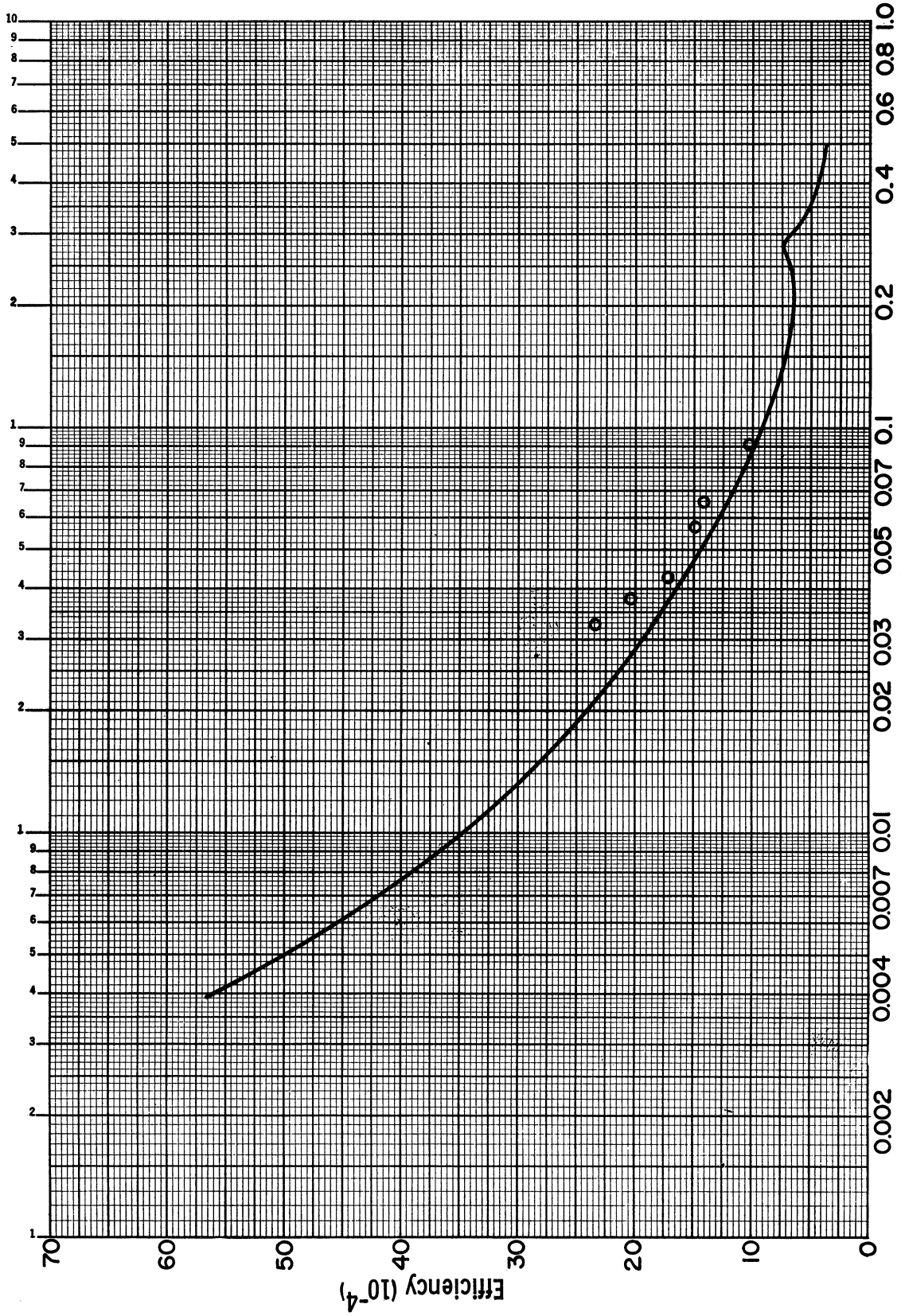

Fig. 10. Monitor efficiency vs. energy.

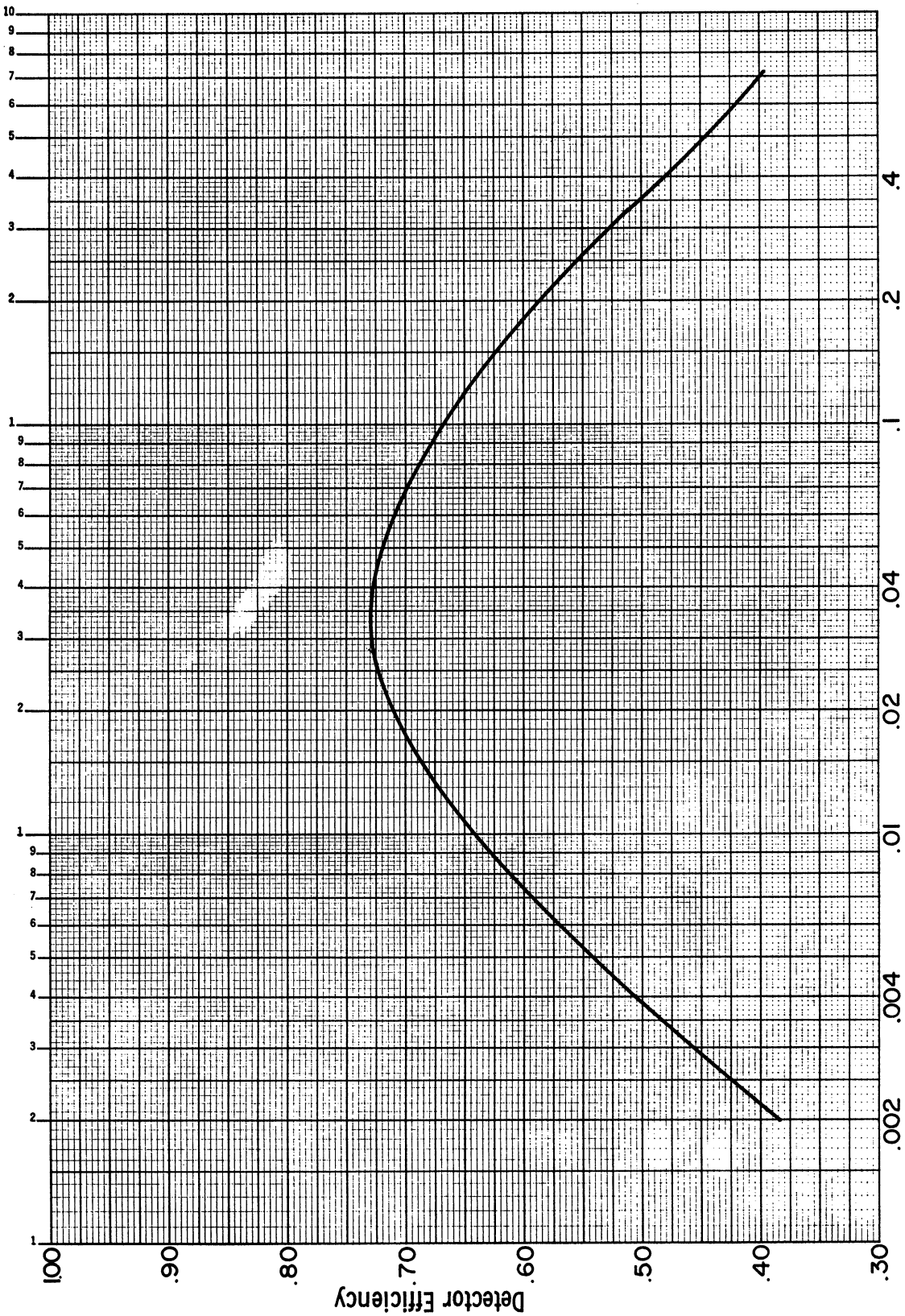

Fig. 11. Scattering detector efficiency vs. energy.

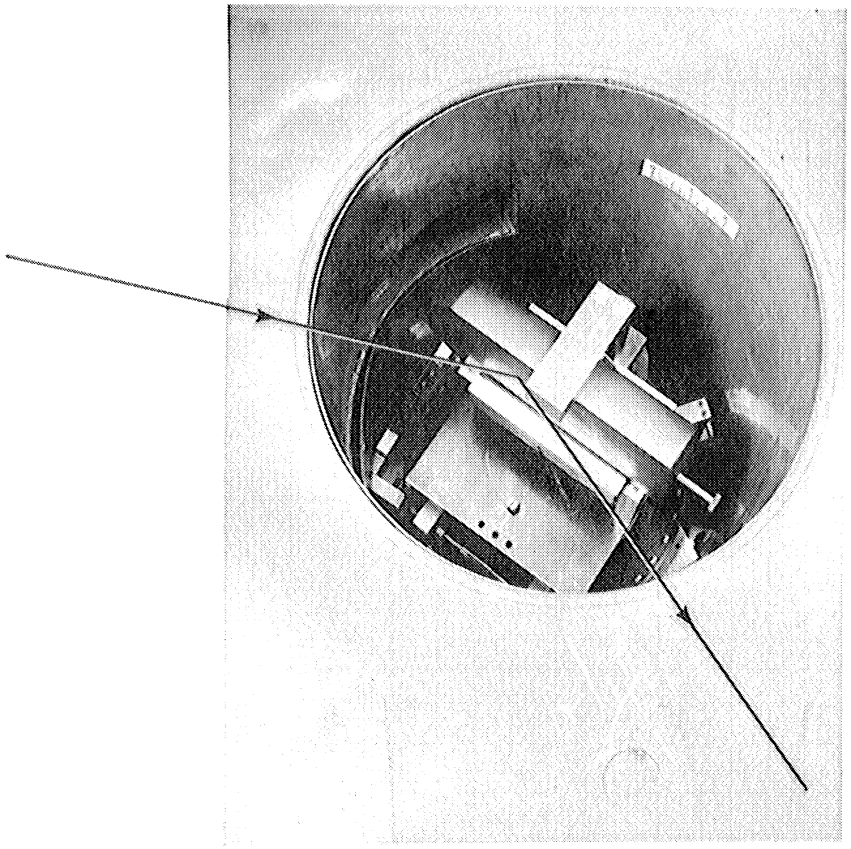

Fig. 12. Cu crystal monochromator.

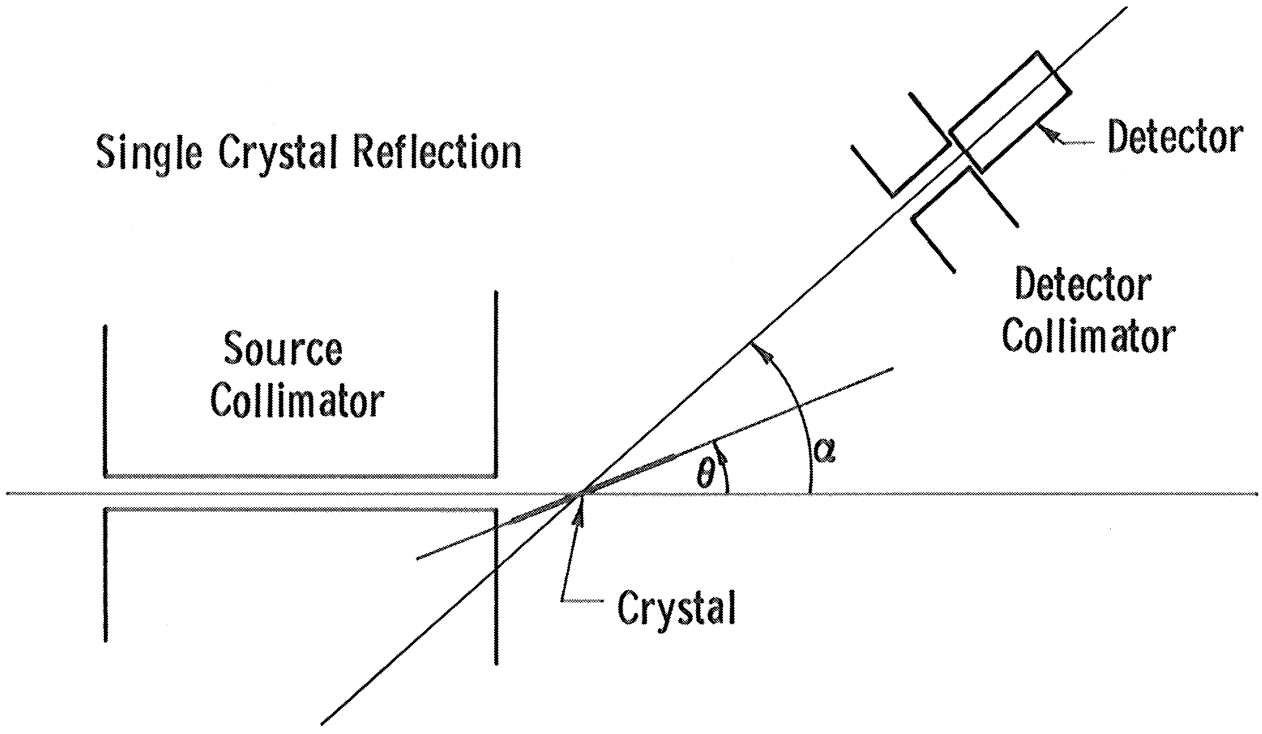

Fig. 13. Experimental arrangement for η measurements.

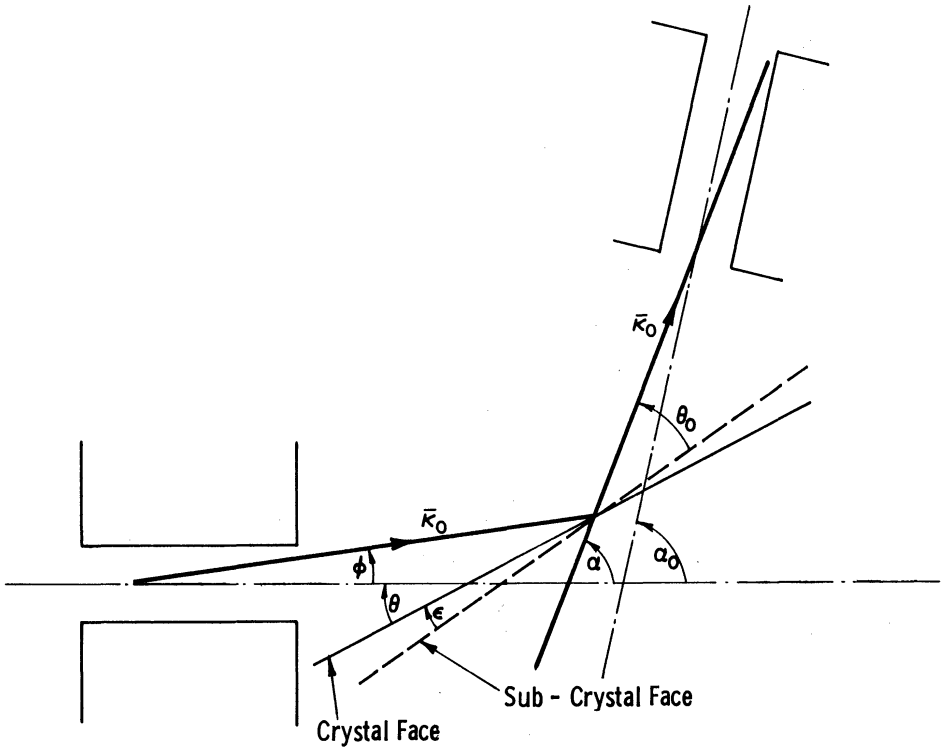

Fig. 14. Angle relationship in η measurements.

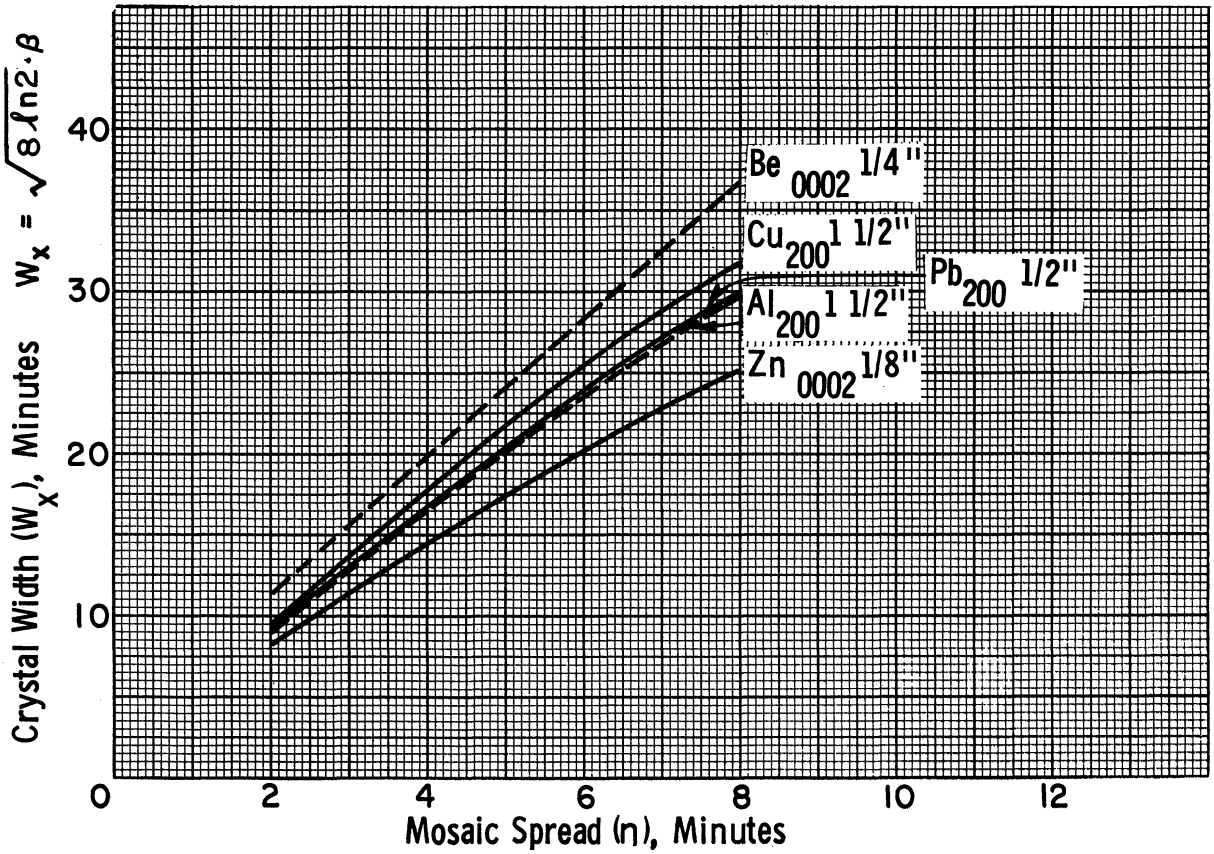

Fig. 15. Calculation of β vs. η for several crystals.

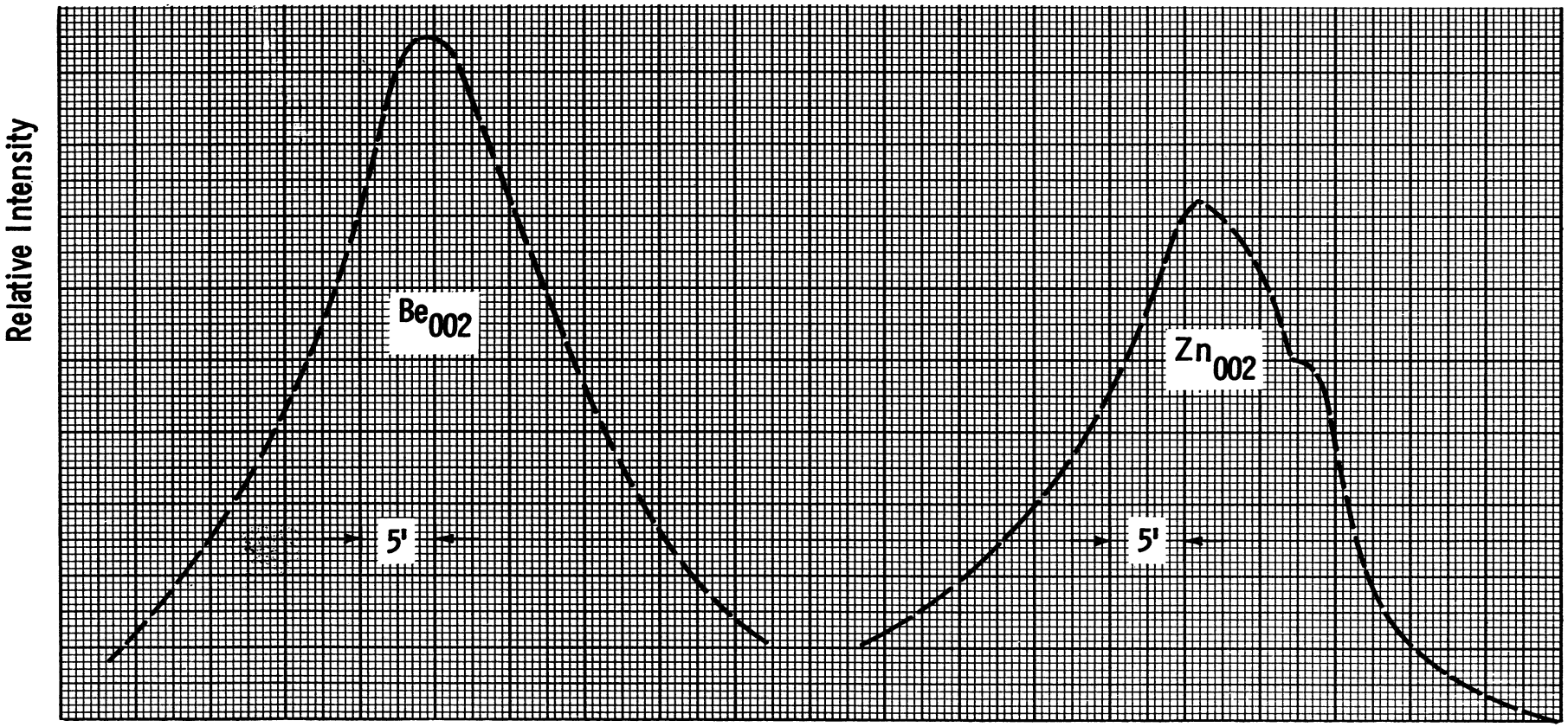

Fig. 16. Single-crystal rocking curves for Be, Zn.

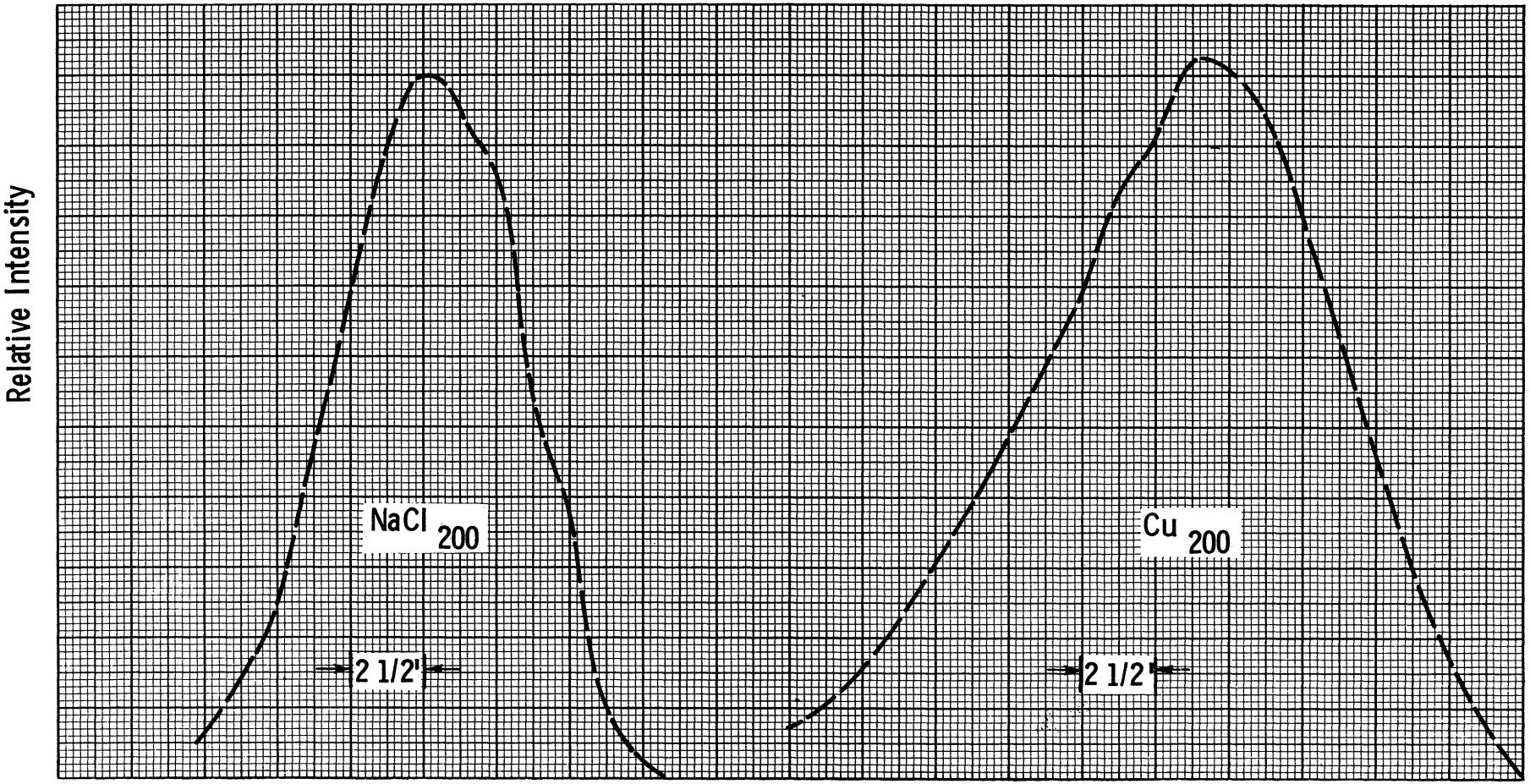

Fig. 17. Single-crystal rocking curves for Cu, NaCl.

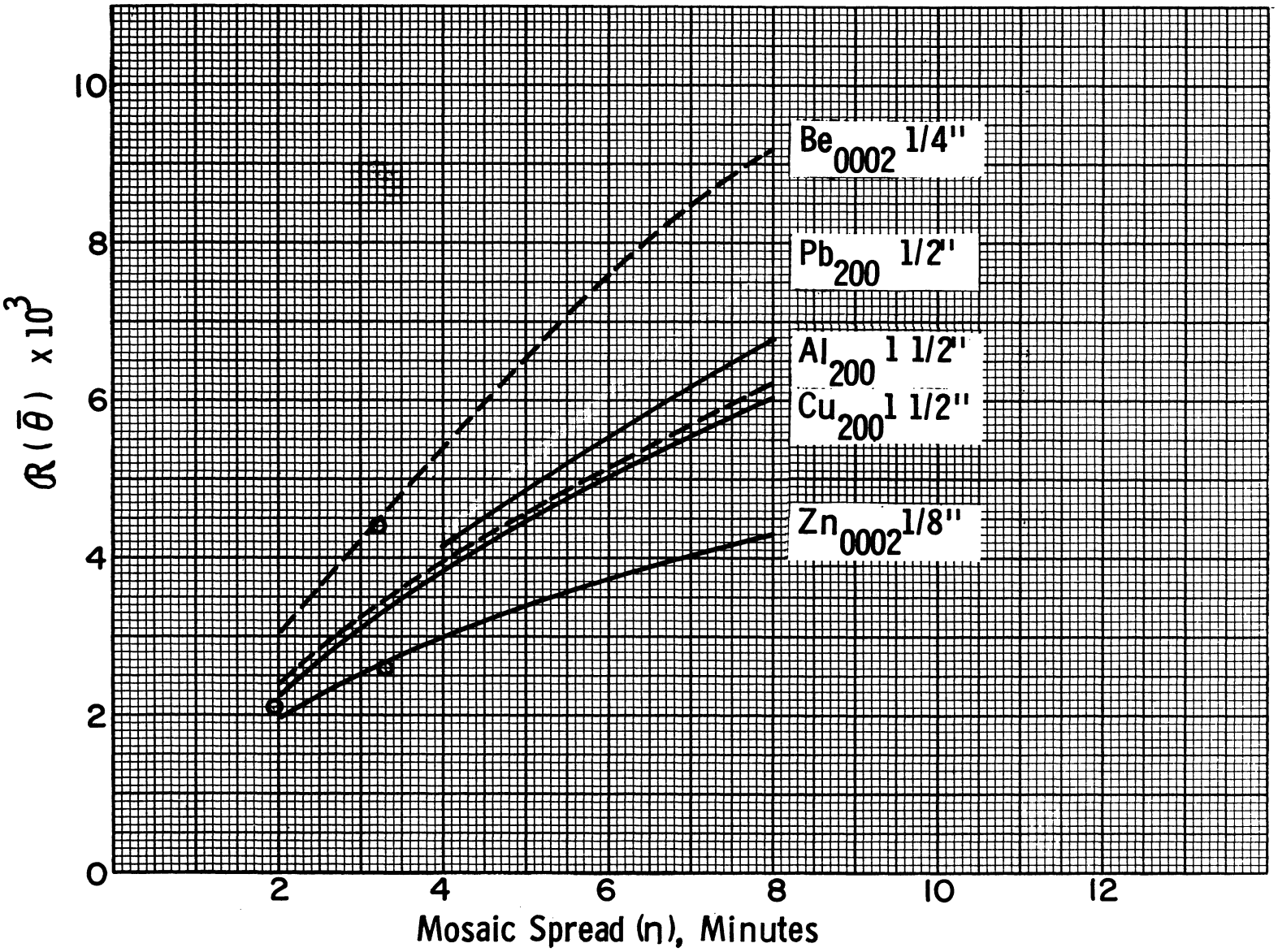

Fig. 18. Calculation of integrated reflectivity vs. η for several crystals.

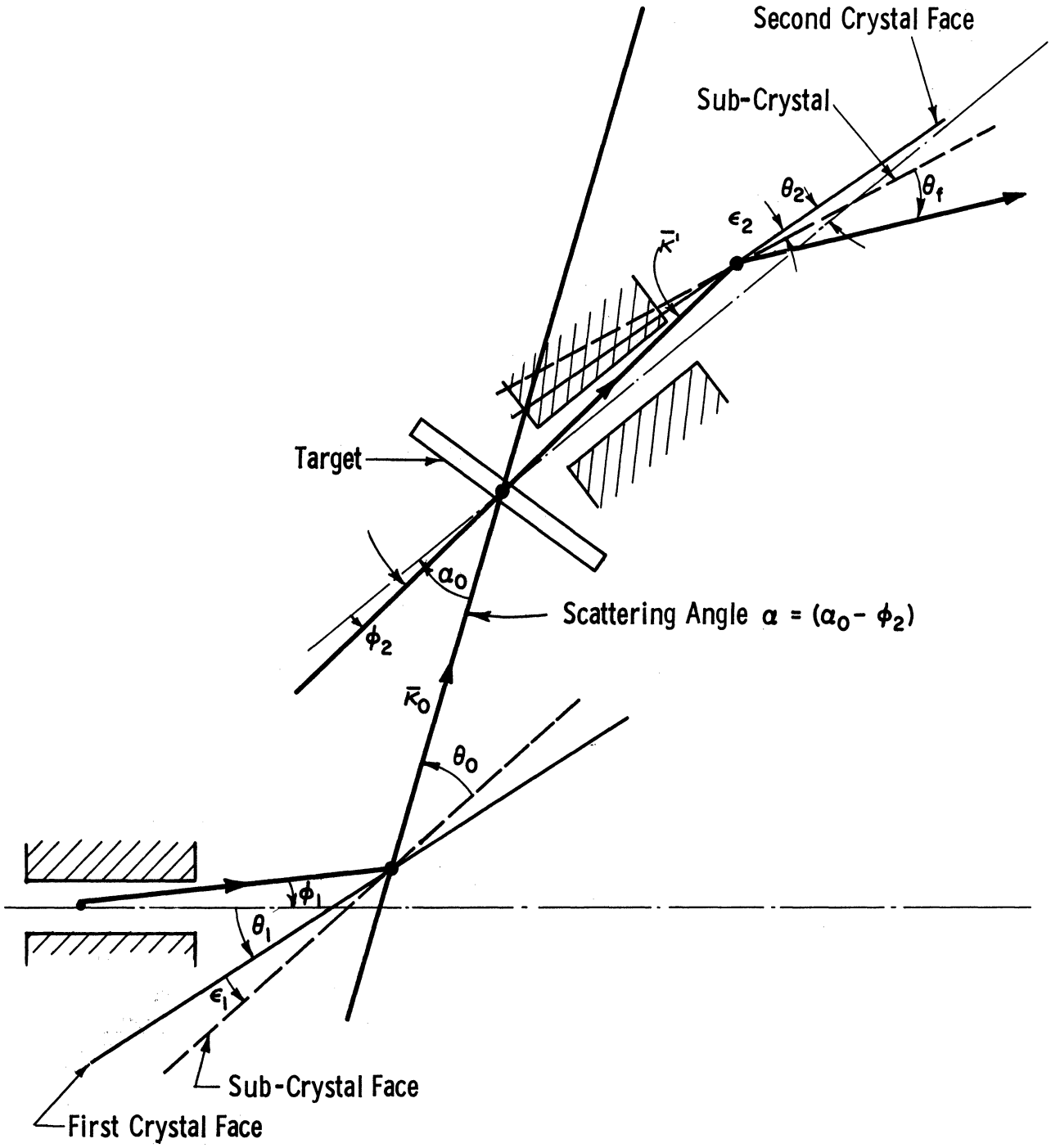

Fig. 19. Angle relationship for triple scattering.

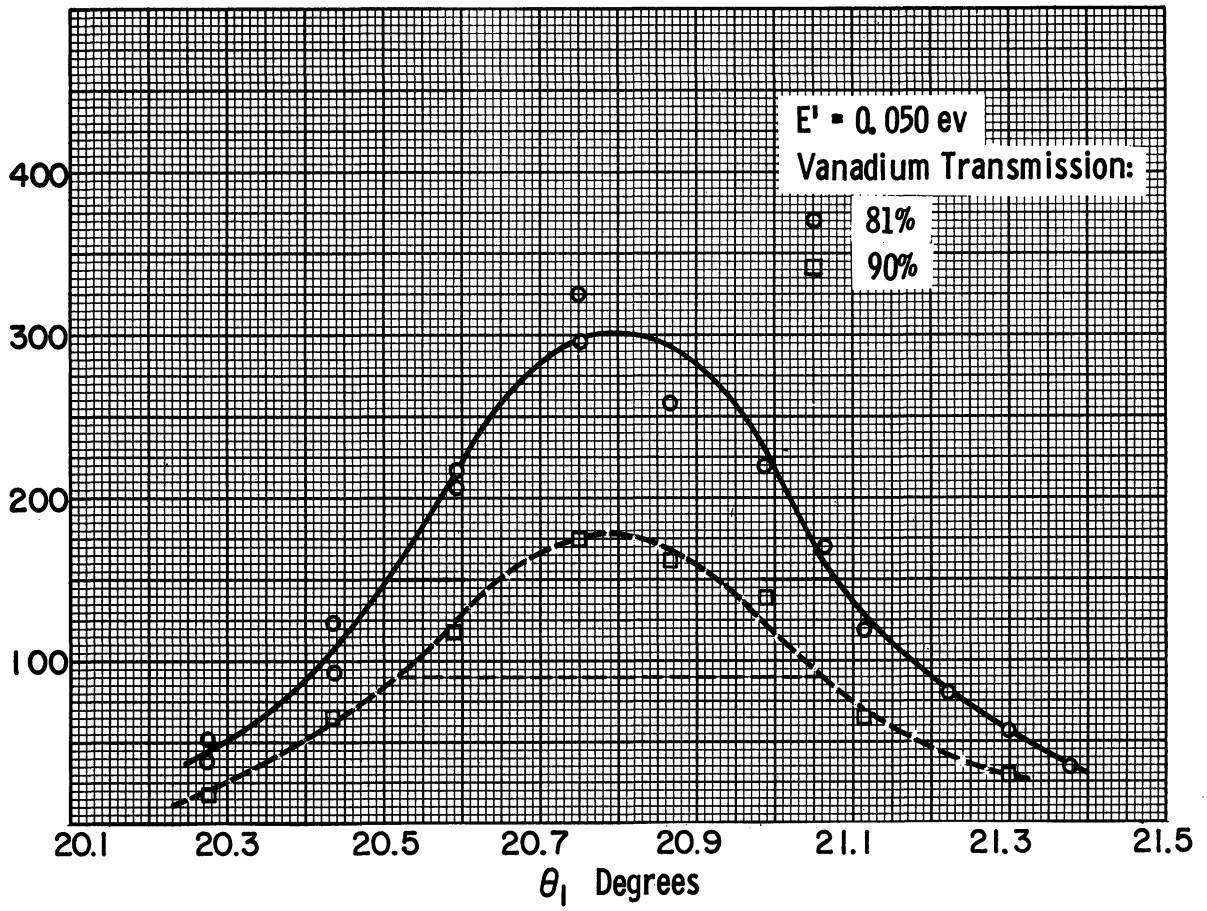

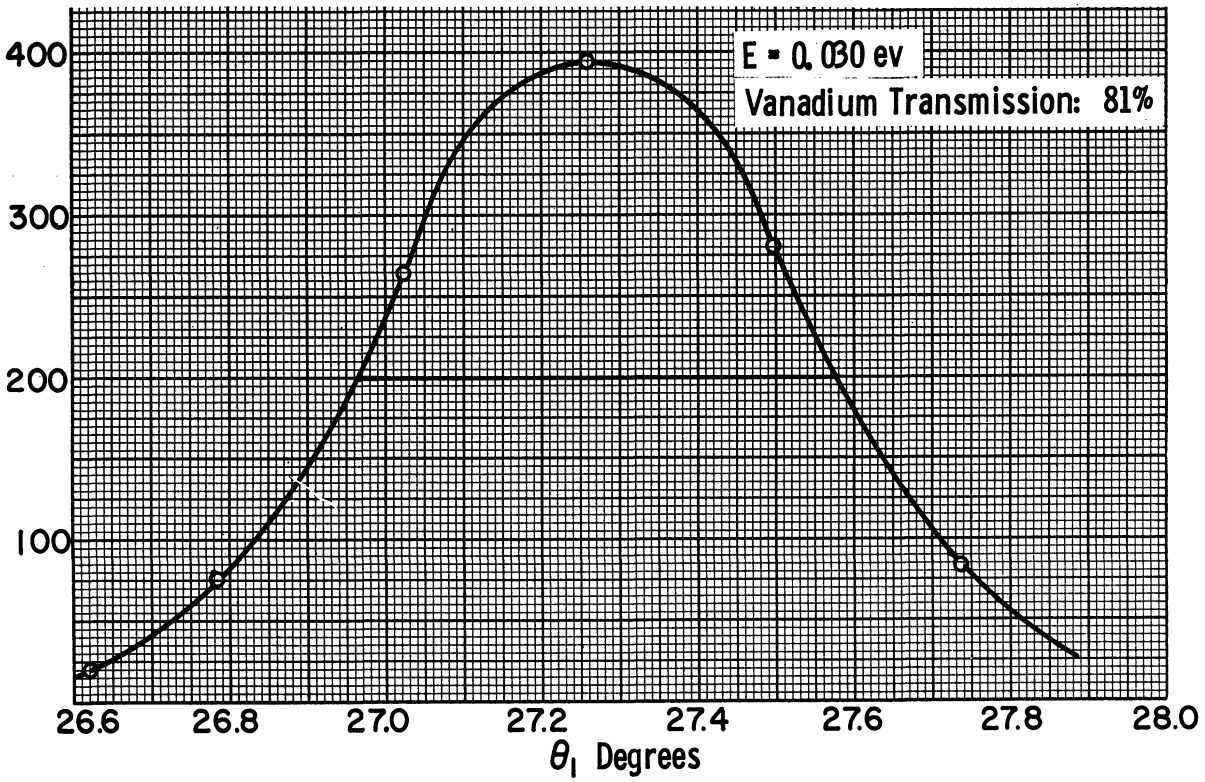

Fig. 20. Resolution measurements at .03, .05 ev.

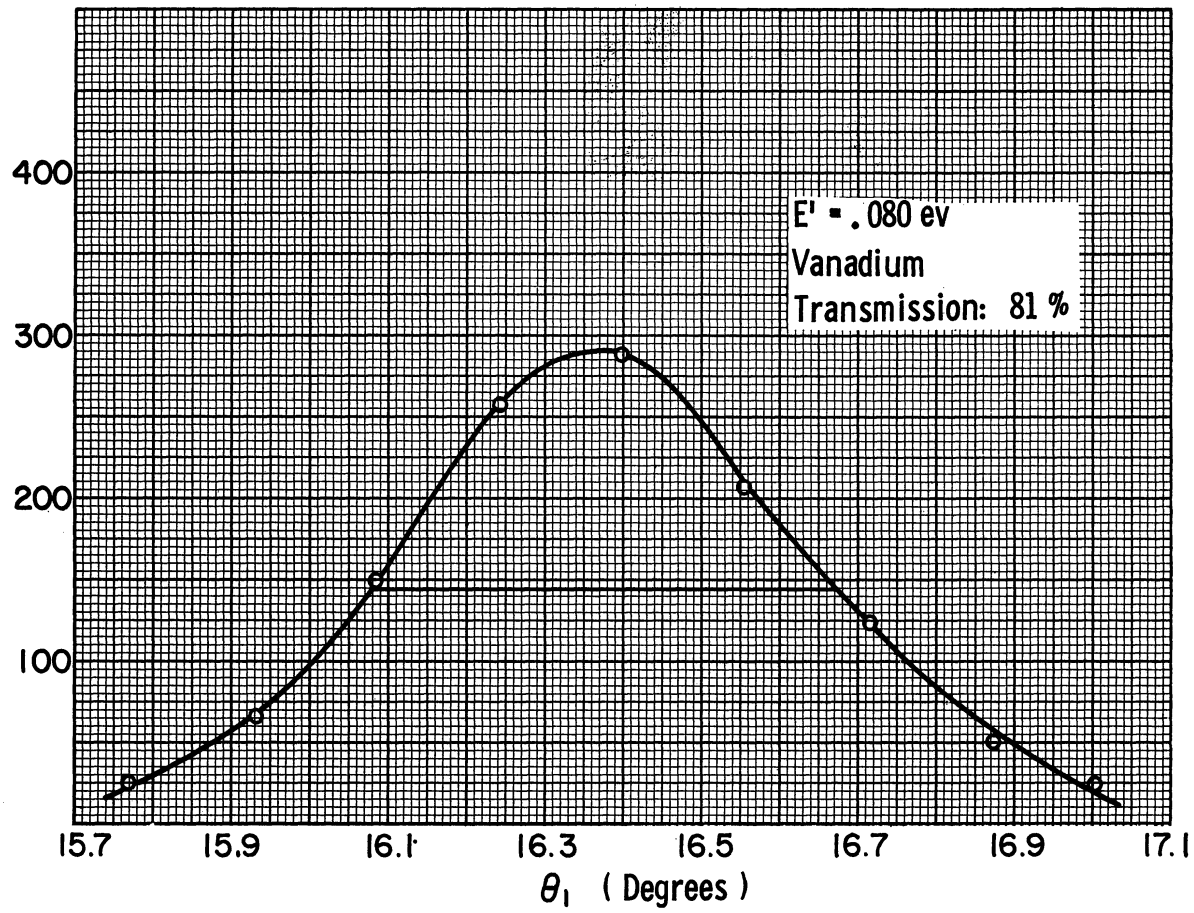

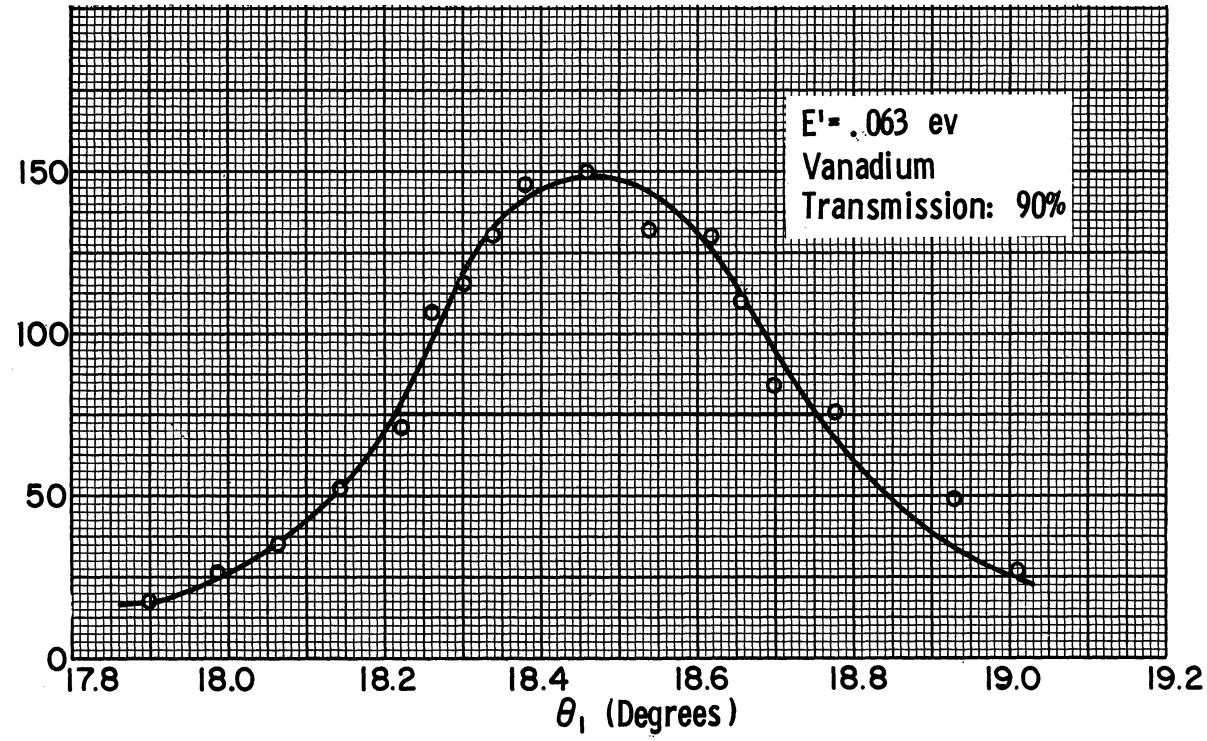

Fig. 21. Resolution measurements at .08, .063 ev.

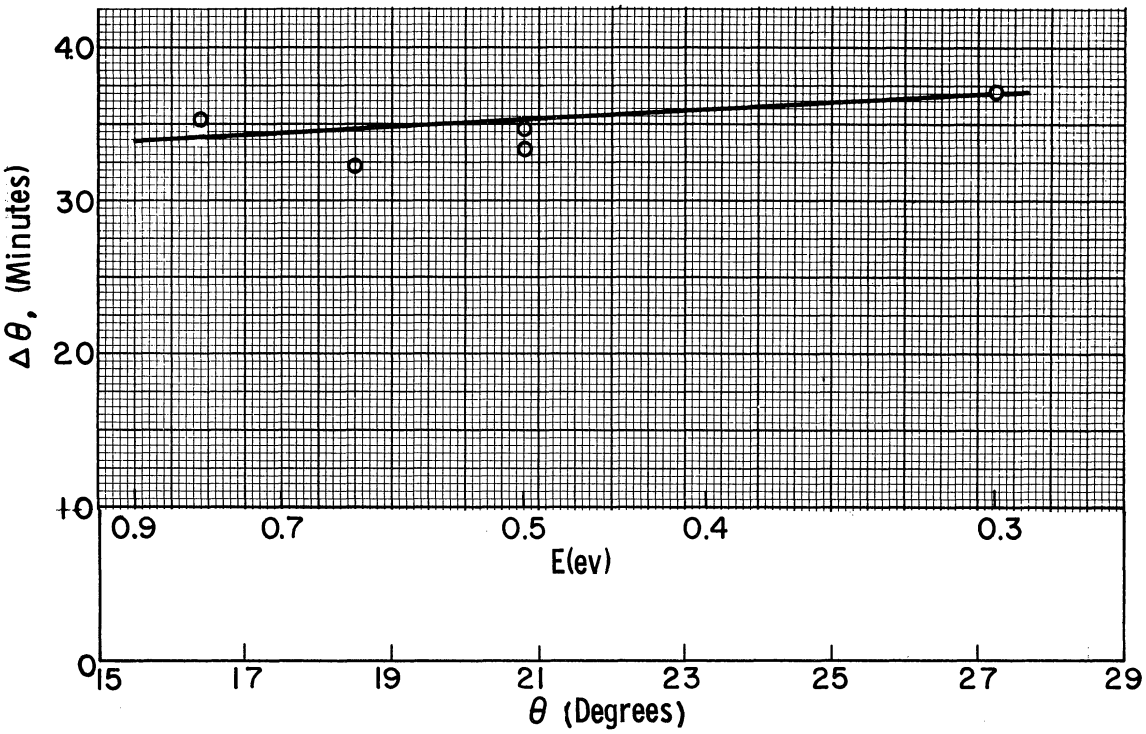

Fig. 22a. Variation in angular width with energy and Bragg angle.

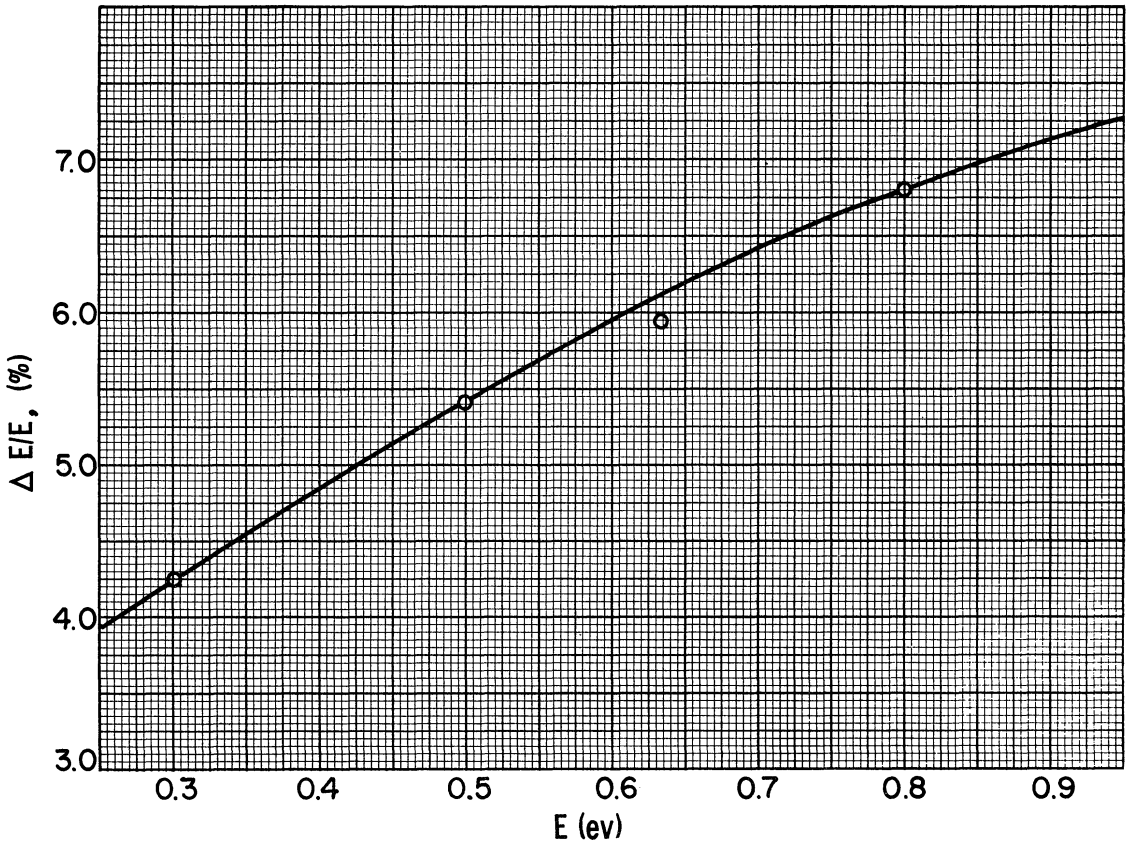

Fig. 22b. Apparent energy resolution vs. energy.

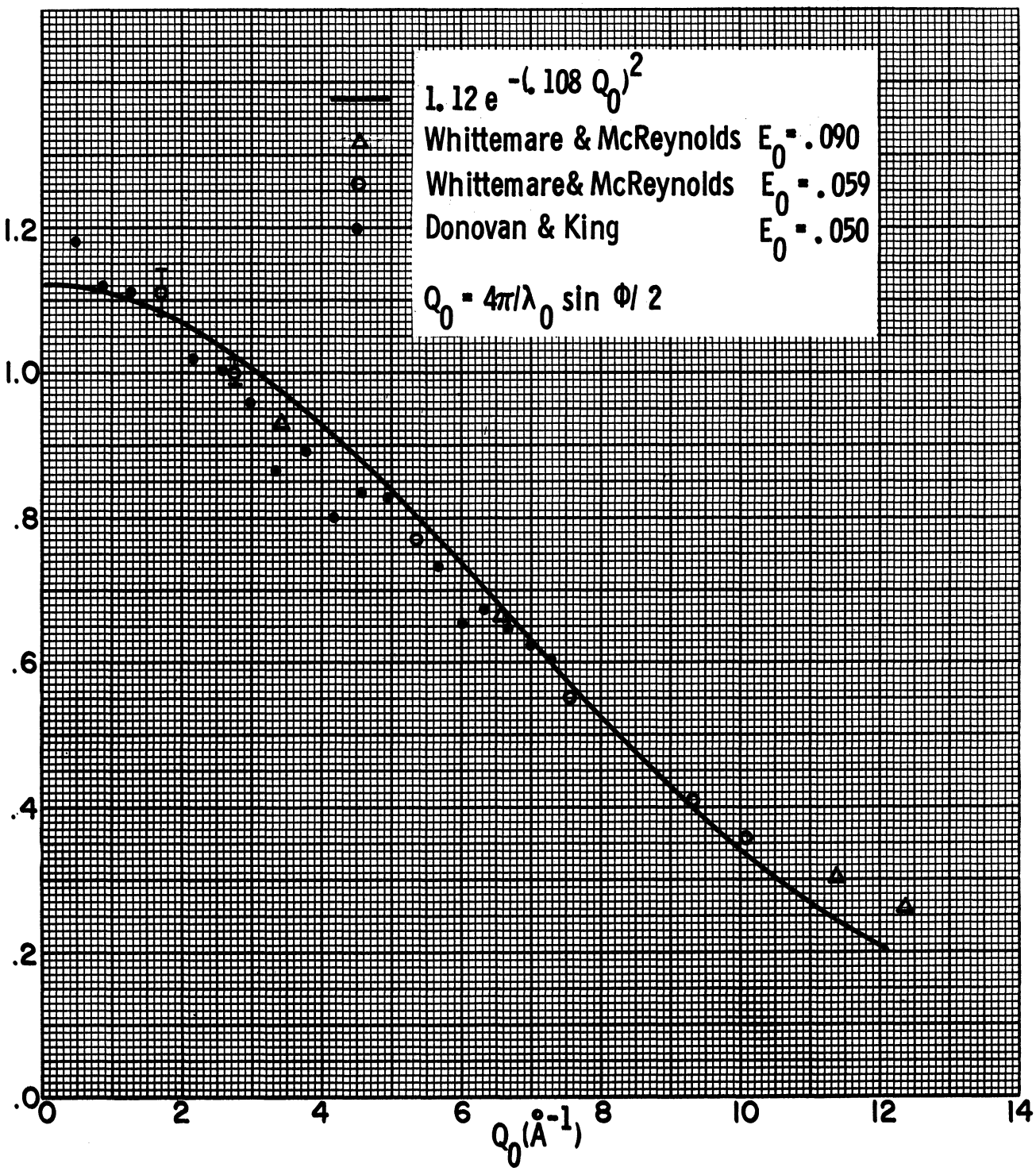

Fig. 23. Angular distribution from C_nH_{2n}.

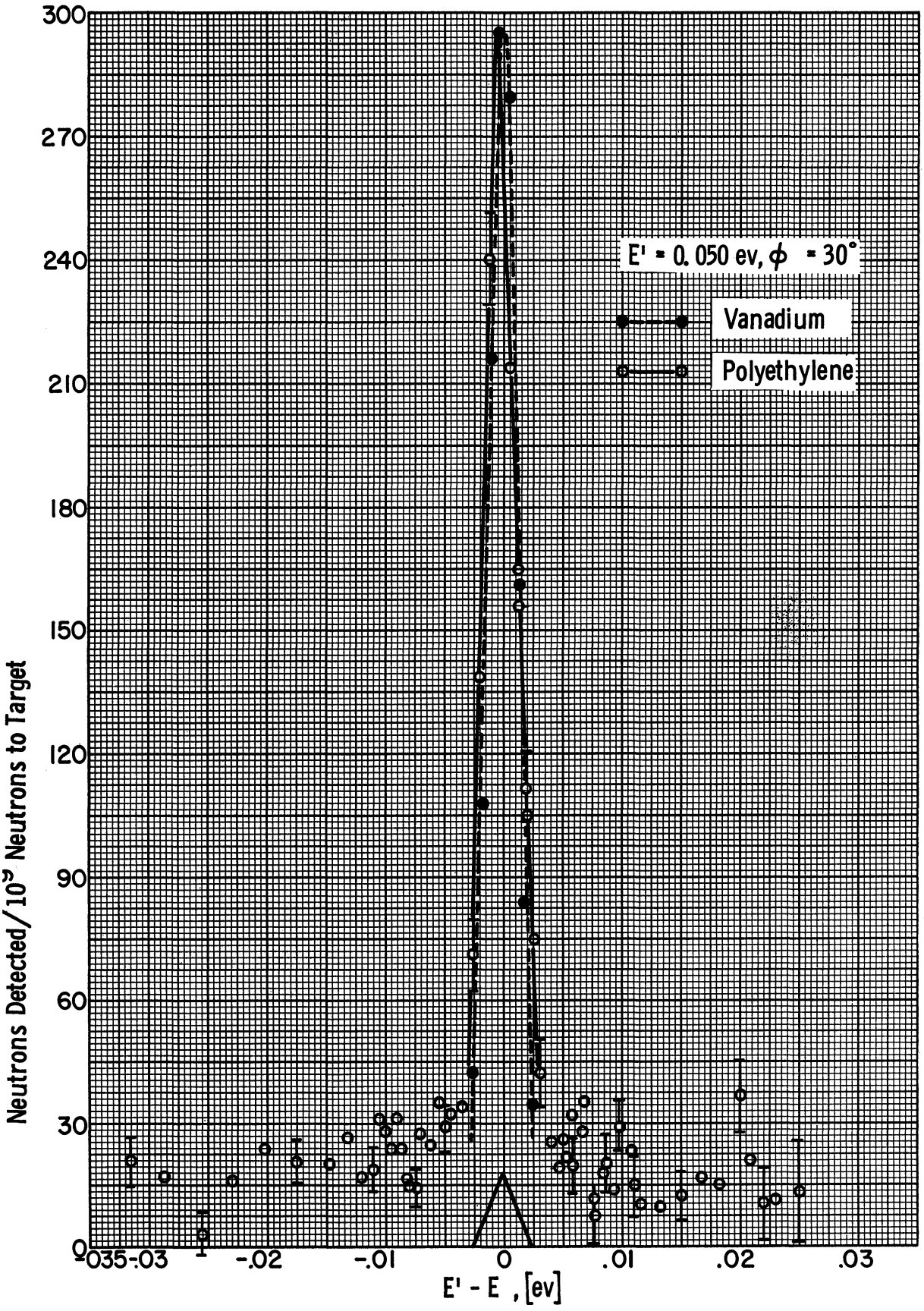

Fig. 24. Differential scattering from C_nH_{2n} at 30° scattering angle.

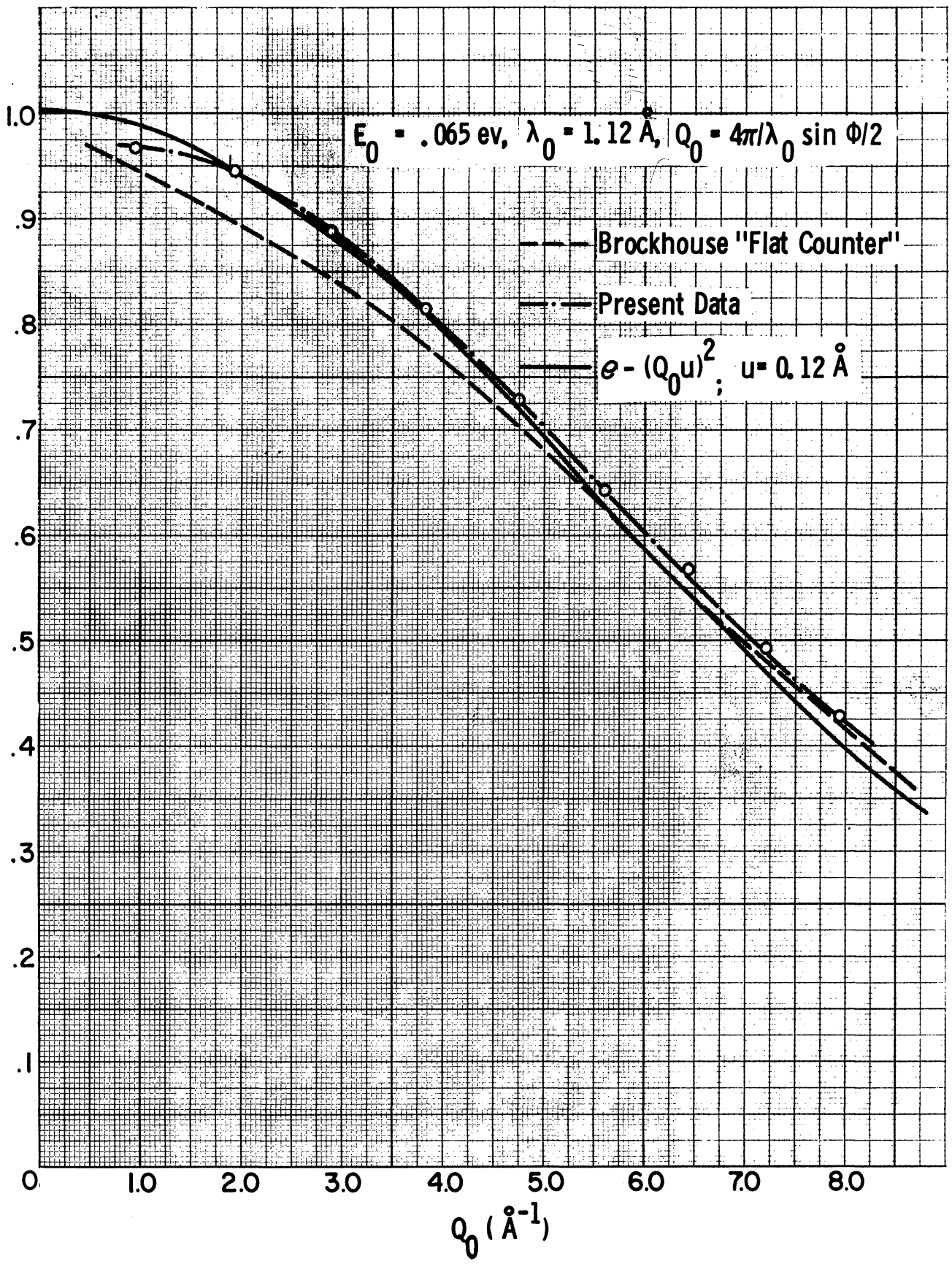

Fig. 25. Angular distribution for H_2O.

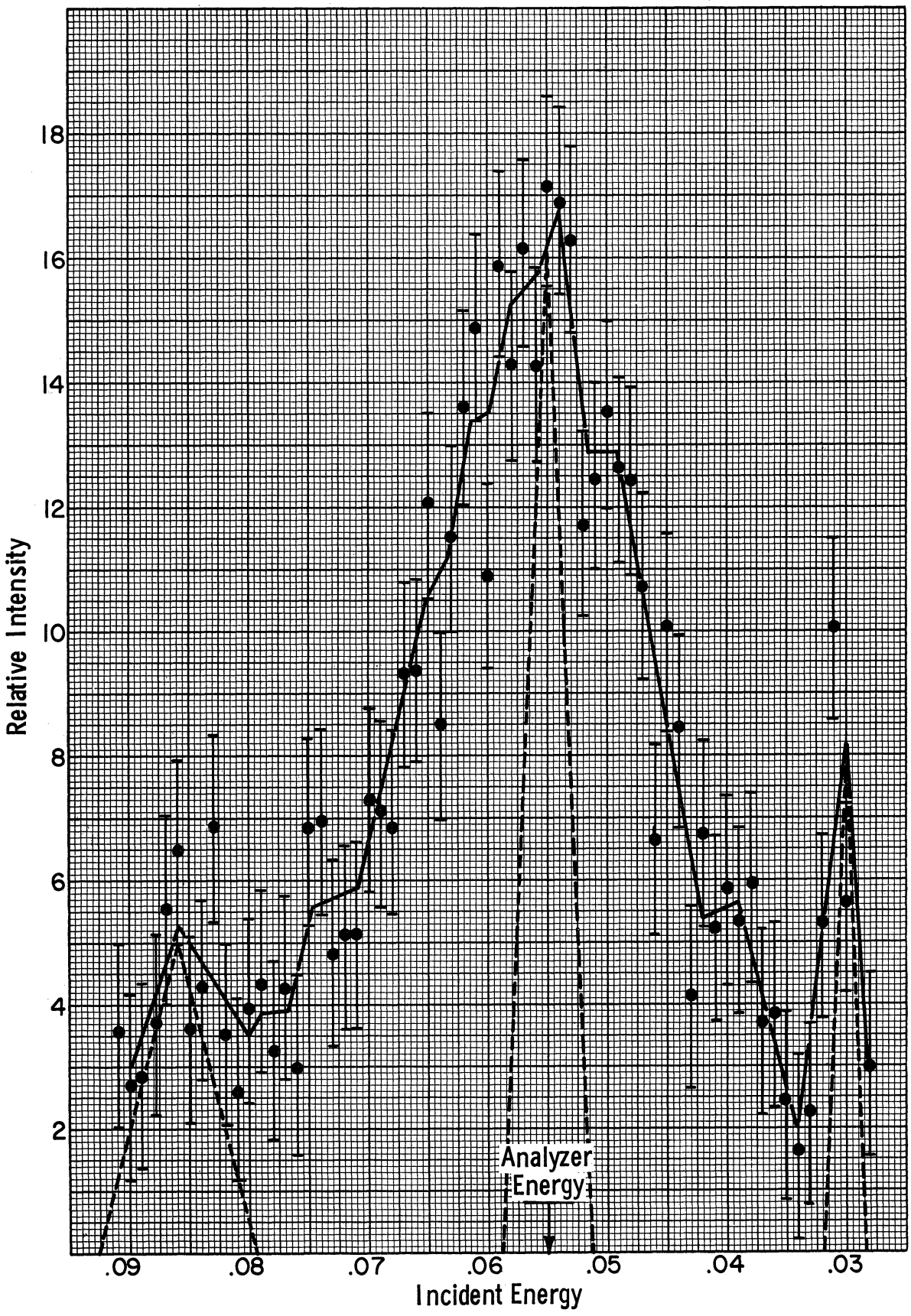

Fig. 26. Differential scattering from H_2O at 70°. (Temperature equals 20°C.)